Atmos. Chem. Phys. Discuss., 9, 3307–3365, 2009
www.atmos-chem-phys-discuss.net/9/3307/2009/

Atmospheric Chemistry and Physics Discussions

This discussion paper is/has been under review for the journal *Atmospheric Chemistry and Physics (ACP)*. Please refer to the corresponding final paper in *ACP* if available.

Sulfur isotope analysis of individual aerosol particles – a new tool for studying heterogeneous oxidation processes in the marine environment

B. W. Sinha[1], P. Hoppe[1], J. Huth[1], S. Foley[2], and M. O. Andreae[3]

[1]Particle Chemistry Department, Max Planck Institute for Chemistry, P.O. Box 3060, 55020 Mainz, Germany
[2]Departent of Geosciences, Johannes Gutenberg University, Joh.-J.-Becher-Weg 21, 55099 Mainz, Germany
[3]Biogeochemistry Department, Max Planck Institute for Chemistry, P.O. Box 3060, 55020 Mainz, Germany

Received: 17 November 2008 – Accepted: 25 November 2008 – Published: 2 February 2009

Correspondence to: B. W. Sinha (winterho@mpch-mainz.mpg.de)

Published by Copernicus Publications on behalf of the European Geosciences Union.

Abstract

Understanding the importance of the different oxidation pathways of sulfur dioxide (SO_2) to sulfate is crucial for an interpretation of the climate effects of sulfate aerosols. Sulfur isotope analysis of atmospheric aerosol is a well established tool for identifying sources of sulfur in the atmosphere and assessment of anthropogenic influence. The power of this tool is enhanced by a new ion microprobe technique that permits isotope analysis of individual aerosol particles as small as 0.5 μm diameter. With this new single particle technique, different types of primary and secondary sulfates are first identified based on their chemical composition, and then their individual isotopic signature is measured. Our samples were collected at Mace Head, Ireland, a remote coastal station on the North Atlantic Ocean. Sea-salt-sulfate (10–60%), ammonium sulfate/sulfuric acid particles (15–65%), and non-sea-salt-sulfate (nss-sulfate) on aged salt particles all contributed significantly to sulfate loadings in our samples.

The isotopic composition of secondary sulfates depends on the isotopic composition of precursor SO_2 and the oxidation process. The fractionation with respect to the source SO_2 is poorly characterized. In the absence of conclusive laboratory experiments, we consider the kinetic fractionation of −9‰ during the gas phase oxidation of SO_2 by OH as suggested by Saltzman et al. (1983) and Tanaka et al. (1994) to be the most reasonable estimate for the isotope fractionation during gas phase oxidation of SO_2 (α_{hom}=0.991) and the equilibrium fractionation for the uptake of SO_2(g) into the aqueous phase and the dissociation to HSO_3^- of +16.5‰ measured by Eriksen (1972a) to be the best approximation for the fractionation during oxidation in the aqueous phase (α_{het}=1.0165). The sulfur isotope ratio of secondary sulfate particles can therefore be used to identify the oxidation pathway by which this sulfate was formed. However, the fraction of heterogeneous and homogeneous oxidation pathway calculated is very sensitive to the isotope fractionation assumed for both pathways. Particles with known oxidation pathway (fine mode ammonium sulfate) are used to estimate the isotopic composition of the source SO_2. It ranged from $\delta^{34}S_{VCDT}$=(0±3)‰

ACPD
9, 3307–3365, 2009

to $\delta^{34}S_{VCDT}$=(14±3)‰ under clean conditions and $\delta^{34}S_{VCDT}$=(3±1)‰ under polluted condition. Condensation of H_2SO_4(g) onto sea salt aerosol produces an isotopic ratio that, when plotted against the sea-salt-sulfate content of the sample, lies on a mixing line between sea salt and ammonium sulfate. The contribution of heterogeneous oxidation is estimated based on the deviation of non-sea-salt-sulfate from this isotopic mixing line.

The contribution of heterogeneous oxidation to nss-sulfate formation on aged sea salt sodium sulfate, magnesium sulfate gypsum and mixed sulfate particles under clean conditions is on average 10% for coarse and 25% for fine mode particles. Under polluted conditions, the contribution of heterogeneous oxidation to nss-sulfate formation increased to 60% on coarse mode and 75% on fine mode particles. However, large day-to-day variations in the contribution of heterogeneous oxidation to nss-sulfate formation occurred. Our results suggest that a significant portion of SO_2 in coastal regions is converted to fine mode ammonium sulfate/sulfuric acid particles (40–80% of nss-sulfate) and that condensation of H_2SO_4(g) contributes significantly even to the nss-sulfate in aged sea salt particles (20–85%).

1 Introduction

Sub-micron sulfate particles are efficient light scatterers and cloud condensation nuclei, and their direct and indirect radiative effects influence the Earth's climate significantly (Charlson et al., 1987; Andreae and Crutzen, 1997; Andreae et al., 2005). Formation and growth of sub-micron sulfate particles generally proceeds by condensation of gaseous sulfuric acid (H_2SO_4(g)) produced by homogeneous gas phase oxidation of SO_2 (Andronache et al., 1997; Kulmala et al., 2000; Weber et al., 2001; O'Dowd et al., 2002). The heterogeneous oxidation of SO_2, on the other hand, tends to enhance sulfate in coarse mode aerosol particles, whose climate impact is limited by their small number, large size, and short atmospheric residence times. Therefore, competition between heterogeneous oxidation and homogeneous oxidation pathways determines

ACPD
9, 3307–3365, 2009

the climate impact of sulfur dioxide emission.

Sulfur dioxide is released as a result of anthropogenic activity (fossil fuel and biomass burning, 60–100 Tg a^{-1}; all values expressed as mass of sulfur) and from natural sources (volcanic gases and dimethyl sulfide (DMS), 20–60 Tg a^{-1}) (Penner et al., 2001). In the atmosphere, SO_2 can be oxidized either via homogeneous oxidation pathways or via heterogeneous oxidation pathways. In homogeneous oxidation, SO_2(g) reacts with gaseous atmospheric oxidants such as OH(g) and forms H_2SO_4(g).

$$SO_2(g) + OH(g) + M \rightarrow HOSO_2(g) + M \quad \text{(R1)}$$
$$HOSO_2(g) + O_2(g) \rightarrow HO_2(g) + SO_3(g)$$
$$SO_3(g) + H_2O(g) + M \rightarrow H_2SO_4(g) + M$$

Heterogeneous oxidation involves dissolution of SO_2 followed by the acid-base dissociation of $SO_2{\cdot}H_2O$(l) to HSO_3^-(l) (pK_{a1}=1.9) and SO_3^{2-}(l) (pK_{a2}=7.2).

Oxidation takes place by dissolved O_3

$$O_3(l) + SO_3^{2-}(l) \rightarrow O_2(l) + SO_4^{2-}(l) \quad \text{(R2)}$$

and dissolved H_2O_2

$$HSO_3^-(l) + H_2O_2(l) \rightarrow SO_2OOH^-(l) + H_2O(l) \quad \text{(R3)}$$
$$SO_2OOH^-(l) + H^+(l) \rightarrow H_2SO_4(l).$$

Heterogeneous oxidation, compared to homogeneous oxidation, occurs rapidly. However, acidification of the aerosol can cause self quenching of (R2), while (R3) is limited by the availability of the oxidant H_2O_2 (Seinfeld and Pandis, 1998). Due to the low pH of cloud water, the oxidation of SO_2 in clouds and fog is dominated by reaction with H_2O_2 (Lelieveld and Crutzen, 1991; Warneck, 1999; Jacob, 2000; Benkovitz et al., 2001). However, for reactions on deliquescent sea salt particles (pH>6) the heterogeneous oxidation of SO_2 by O_3 is 10^5 times faster than that the reaction with H_2O_2 (Seinfeld and Pandis, 1998). Therefore, deliquescent sea salt particles may be

an important medium for the oxidation of sulfuric acid (Suhre et al., 1995; Andreae and Crutzen, 1997; Sievering et al., 1999; Bauer and Koch, 2005).

Oxidants other than OH, O_3, and H_2O_2 are usually considered to be of little importance on a global scale. However, previous research at Mace Head has shown that measured gas phase sulfuric acid concentrations (H_2SO_4(g)) cannot be explained by measured SO_2(g) and OH(g) concentrations (Berresheim et al., 2002). This agrees well with results of the comparison of large-scale sulfate aerosol models study (COSAM), which showed that on average models overestimate SO_2(g) by a factor of 2 and underestimate SO_4^{2-} by 20% (Barrie et al., 2001). Berresheim et al. (2002) suggested additional pathways for gas phase oxidation of SO_2 possibly via a stable Criegee biradical formed during the ozonolysis of unsaturated hydrocarbons, which may then oxidize SO_2 to H_2SO_4 (Cox and Penkett, 1971; Horie and Moortgat, 1991). Alternatively, a DMS oxidation pathway leading directly to the formation of SO_3 has been suggested (Berresheim et al., 2002; O'Dowd et al., 2002).

Several studies have investigated the chemical composition of marine aerosol particles using individual particle analysis methods near Europe (Hoornaert et al., 1996; Ebert et al., 2000; Ebert et al., 2002; Rojas and van Grieken, 1992), the Canary Islands (Posfai et al., 1995; Hoornaert et al., 2003; Li et al., 2003) and in the southern Atlantic (Niemi et al., 2005), and discussed the importance of different oxidation pathways based on chemical evidence (Posfai et al., 1995; Sievering et al., 1999). The mass independent signature of oxygen isotope ratios has recently been used to quantify the importance of the O_3 oxidation pathway of SO_2 in the Indian Ocean (Alexander et al., 2005). This pathway reportedly decreased gas phase SO_2 concentrations and increased H_2SO_4 production rates by 10–30%.

While the mass independent fractionation of oxygen isotope ratios is a valuable tool to trace the overall importance of the O_3 pathway for the oxidation of sulfur dioxide (Alexander et al., 2005), the new ion microprobe technique for sulfur isotope analysis of individual aerosol particles (Sinha et al., 2008) permits estimation of the total contribution of heterogeneous oxidation to the formation of non-sea-salt-sulfate (nss-

sulfate). Moreover, a single particle approach is the only way to elucidate why and under which conditions certain particles serve as surfaces for heterogeneous reactions, thereby enabling us to predict future changes in oxidation pathways. Our study combines chemical, morphological and sulfur isotopic information of individual aerosol particles, permitting the study of the oxidation pathway of nss-sulfate in different types of sulfate aerosol particles. To introduce the concept of using sulfur isotope ratios to establish oxidation pathways of sulfur in the marine atmosphere, Sect. 2 gives a short introduction to the isotope chemistry of sulfur. Details of the measurement technique and data analysis are described in Sect. 3 and results are presented in Sect. 4.

2 Isotope chemistry of sulfur in the marine atmosphere

Primary sulfate particles, such as sea salt, mineral dust or fly ash, are directly emitted in the form of SO_4^{2-}, while secondary sulfates are formed by the oxidation of SO_2 in the atmosphere. While the isotopic composition of primary sulfate can be interpreted directly as a source signature, conversion of gaseous SO_2 to sulfate introduces further changes to the isotopic composition (Thode et al., 1945; Eriksen, 1972a,b; Saltzman et al., 1983; Tanaka et al., 1994; Leung et al., 2001), which can be used to study oxidation pathways, provided the isotopic composition of the source SO_2 and fractionation during oxidation is known (Fig. 1).

Sulfur isotope ratios are expressed in delta notation defined according to the equation given below (VCDT: Vienna Canyon Diablo Troilite, i.e., deviation from solid troilite reference material)

$$\delta^{34}\mathrm{S} = \delta^{34}\mathrm{S}_{VCDT} = \frac{(n(^{34}\mathrm{S})/n(^{32}\mathrm{S}))_{Sample}}{(n(^{34}\mathrm{S})/n(^{32}\mathrm{S}))_{VCDT}} - 1 \quad (1)$$

$(n(^{34}\mathrm{S})/n(^{32}\mathrm{S}))_{VCDT} = 0.044163$ (Ding et al., 2001)

The two most important sources of sulfur in the marine atmosphere are sea salt, and SO_2 derived from the oxidation of DMS. The isotopic composition of modern day

ACPD
9, 3307–3365, 2009

ocean water is δ^{34}S=(20.7±0.3)‰ (Krouse and Grinenko, 1991), but during fractional crystallization of sea salt minor fractionations do occur. Gypsum or anhydrite is slightly enriched (0–2‰) in ^{34}S compared to the seawater from which it has been precipitated. Sulfates precipitated with more soluble halite (NaCl) or potash-magnesia species are depleted in ^{34}S by as much as 4‰ since progressive crystallization of sulfates enriched in ^{34}S depletes the residual droplet (Raab and Spiro, 1991). The isotopic composition published for nss-sulfate produced by the oxidation of DMS ranges from +14 to +22‰ (Calhoun et al., 1991; McArdle and Liss, 1995; McArdle et al., 1998; Patris et al. 2000a,b). Kinetic isotope effects of the DMS+OH reaction to form SO_2 have not been measured, but direct measurements of methanesulfonic acid (MSA) collected over the North Pacific (δ^{34}S=(17.4±0.7)‰; Sanusi et al., 2006) lie well within the range of DMS and H_2S emission deriving from decay of phytoplankton (δ^{34}S=0‰ to 20‰; Krouse and Grinenko, 1991) and suggest that the fractionation is minor. The oxidation of H_2S shows a fractionation of 2 to 3‰, in which SO_2 is enriched in ^{32}S relative to the reactant H_2S (Krouse and Grinenko, 1991).

Anthropogenic SO_2 contributes significantly to SO_2 concentrations even over remote parts of the North Atlantic (Benkovitz et al., 2001; Barrie et al., 2001). The isotopic signature of such emissions can cover a wide range (δ^{34}S=−40‰ to +30‰), but the typical isotopic composition of anthropogenic SO_2 falls within a much narrower range close to 0‰ (flue gas from coal combustion δ^{34}S=−1‰ to +3‰; combustion and refining of oil δ^{34}S∼+5‰; roasting of sulfide ores δ^{34}S∼+3‰; Nielsen, 1974; Krouse and Grinenko, 1991).

Secondary sulfates are formed by the oxidation of SO_2 and the oxidation process alters the isotopic signature (Fig. 1; Thode et al., 1945; Eriksen, 1972a,b; Saltzman et al., 1983; Tanaka et al., 1994). Saltzman et al. (1983) and Tanaka et al. (1994) determined the isotopic fractionation (α_{hom}) for gas phase oxidation of SO_2 by OH as being kinetically driven. Tanaka et al. (1994) calculated a fractionation of −9‰ (α_{hom}=0.991, $^{34}S/^{32}S_{fractionation}=(\alpha - 1)$) using ab initio quantum mechanical calculations. In contrast, Leung et al. (2001), using RRKM (Rice, Ramsperger, Kassel, and Marcus) tran-

ACPD
9, 3307–3365, 2009

sition state theory, calculated the fractionation as an inverse kinetic isotope effect, with $^{34}SO_2$ reacting faster than $^{32}SO_2$ resulting in a $\delta^{34}S$ increase of 140‰ (α_{hom}=1.14) under atmospheric conditions.

At first sight, the fractionation calculated by Leung et al. (2001) agrees well with measurements of stratospheric sulfate (Castleman et al., 1974). The data of Castleman et al. (1974) seemed to indicate that during the oxidation of SO_2 to sulfate in the stratosphere following the Mt. Agung eruption, Rayleigh fractionation occurred with ^{34}S being enriched in sulfate and SO_2 depleted in ^{34}S. However, recent research has shown that following the volcanic eruption a separation of the sulfur into two reservoirs carrying a mass independent isotope fractionation with opposing signs took place (Baroni et al. 2007) and UV induced photo oxidation has been suggested to explain the mass independent signature. Since the oxidation of SO_2 by OH is not responsible for the mass independent signature observed in the sulfate during the time period in question, this reaction is not the only reaction dominating the isotopic signature of the sulfate. Therefore, the simple Rayleigh fractionation during oxidation of SO_2 by OH proposed by Leung (2001) can no longer be used to interpret the dataset.

Currently, the best way to estimate the fractionation of the gas phase and aqueous phase oxidation is to look at seasonal trends in the isotopic composition of simultaneously collected SO_2 and SO_4^{2-} and to evaluate the equation $(\delta^{34}S_{SO_4^{2-}}-\delta^{34}S_{SO_2})=(1+\delta^{34}S_{SO_2})\cdot[(1-f_{hom})\cdot\alpha_{het}+f_{hom}\cdot\alpha_{hom}]-1$ for different seasons. The contribution of the gas phase oxidation (f_{hom}) varies from 0% (nighttime, arctic winter) to roughly 60% (noon/early afternoon on a bright summer day) of the total sulfate formed. Therefore, during winter more sulfate should be formed through oxidation in the aqueous phase, while during summer the importance of gas phase oxidation by OH should increase. The seasonal trends of the isotopic composition of simultaneously collected SO_2 and sulfate allow an estimate of the direction of the isotopic fractionation involved in both pathways. It has been observed that during summer months (more gas phase oxidation) the difference in the $\delta^{34}S$ of SO_2 and sulfate ($\delta^{34}S_{SO_4^{2-}}-\delta^{34}S_{SO_2}$) is generally lower than during winter months (more aqueous phase oxidation) (Saltzmann

et al., 1983; Mukai et al., 2001, Kawamura et al., 2001; Tichomirowa, unpublished data). Occasionally, the sulfate is depleted in ^{34}S compared to the SO_2 during summer months. The same holds for the comparison of the isotopic composition of throughfall (wet deposition of sulfate plus SO_2 from dry deposition on the leaves) and bulk precipitation (Groschekova et al. 1998; Novak et al. 2000, Zhang et al. 1998) with the throughfall occasionally showing a higher $\delta^{34}S$ than the bulk precipitation at the same site during summer months. Even when only one of the species (SO_4^{2-} or SO_2) was collected the seasonality encountered is similar for most sites in the northern hemisphere. In winter the $\delta^{34}S$ of bulk sulfate increases, compared to the summer values at the same site (Caron et al., 1986; Niagru et al., 1987; Ohizumi et al., 1997; Alewell et al., 2000; Ohizumi et al., 2001). On the contrary, the $\delta^{34}S$ of the remaining SO_2 during winter is typically lower than during summer (Novak et al. 2001). This is in line with an enrichment of the heavier isotope in the sulfate due to the increased importance of the aqueous phase oxidation in the winter months and depletion of the SO_2. These seasonal trends support $\alpha_{het}>1$ for the aqueous oxidation pathway. The fact that $\delta^{34}S_{SO_4^{2-}} - \delta^{34}S_{SO_2}$ and $\delta^{34}S$(bulk precipitation)$-\delta^{34}S$(throughfall) is sometimes negative during summer months supports $\alpha_{hom}<1$ for the gas phase oxidation.

In the absence of any conclusive laboratory experiments the seasonality of the sulfur isotopic composition is the best way to estimate the direction of the isotopic fractionation during gas phase oxidation and aqueous phase oxidation. The numbers associated with both processes are far from certain. For the heterogeneous oxidation pathway only the fractionation during the uptake of SO_2 into the aqueous phase and the dissociation to HSO_3^- has been determined, that too under equilibrium conditions (α_{het}=1.0165; Eriksen, 1972a,b). The effect of the terminating reactions has never been properly assessed experimentally and equilibrium is typically not reached under atmospheric conditions. In the aqueous phase, S(IV) is oxidized mainly by H_2O_2 and O_3. Oxidation by other oxidants such as O_2 in the presence of Fe(III) and Mn(II) (Jacob and Hoffmann, 1983), NO_2 (Lee and Schwartz, 1982), NO_3 (Feingold et al., 2002) and HNO_4 (Warneck, 1999; Dentener et al., 2002), and HOCl and HOBr (Vogt et al., 1996;

ACPD
9, 3307–3365, 2009

von Glasow et al., 2002; von Glasow and Crutzen, 2004) are considered to be of minor importance. Further unknown fractionations associated with the oxidation are considered to be negligible compared to the huge equilibrium isotope effect isotope effect during SO_2 dissolution. For O_3, H_2O_2 and metal-catalyzed oxidation as the terminating steps, Saltzman et al. (1983) determined a very small kinetic isotope effect (α=0.999). Therefore, ^{34}S is favored due to the high equilibrium isotope effect, giving SO_4^{2-}(l) an isotopic composition of $\alpha \cong 1.016$ in comparison to source SO_2(g). This happens irrespective of the agent involved in oxidizing the SO_2(l). As a result, sulfur isotope analysis can estimate the importance of all heterogeneous oxidation pathways combined, and does not require any knowledge of the oxidizing agent. The fractionation of the gas phase oxidation pathway (α_{hom}) has not been determined experimentally at all. Additionally, recent research has shown that a significant portion of SO_2 oxidation in particular in coastal regions is not well understood (Barrie et al., 2001; Berresheim et al., 2002). This presents a major uncertainty, as the fractionation of an unknown gas phase oxidation mechanism cannot be included into the isotope mass balance. The absence of laboratory experiments that include the net effect of the reaction for both the formation of sulfate in the gas phase as well as for the aqueous phase oxidation makes the data interpretation a challenging task. Based on current scientific understanding, we consider the kinetic fractionation during the gas phase oxidation of SO_2 by OH as suggested by Saltzman et al. (1983) and Tanaka et al. (1994) to be the most reasonable estimate for the isotope fractionation during gas phase oxidation of SO_2 (α_{hom}=0.991) and the equilibrium fractionation for the uptake and dissociation measured by Eriksen (1972a) the best approximation for the fractionation during oxidation in the aqueous phase (α_{het}=1.0165).

ACPD
9, 3307–3365, 2009

3 Methods

3.1 Sample collection and site description

Samples were collected on a small tower (height 10 m) at the shore laboratory of the Mace Head atmospheric research station at (53°19′34″ N 9°53′14″ W) of the University of Galway. The shore laboratory is 5 m above mean sea level and is at a distance of around 50 m from the shore in the wind direction sector circa 180°to 330°(S-NW). The terrain is mostly low-lying and undulating, the soil is predominantly peat covered by rough grasses, with a significant amount of exposed granite rock. A detailed description of the site has been published by O'Dowd et al. (2002). Samples were collected for a duration of ∼24 h per sample with a stacked filter unit, on gold coated 47-mm-diameter Nuclepore® polycarbonate filters of pore sizes 8 µm (coarse fraction) and 0.4 µm (fine fraction). The cut-off between the coarse and fine fractions was approximately at 2 µm aerodynamic diameter (Table 1). The aerosol was dried by a dryer mounted in the sampling line in front of the stacked filter unit. After sample collection, the filters were placed in individual Petri-slides, wrapped in aluminium foil and stored in a dry vacuum chamber. Before SEM and SIMS analysis, filters were coated with gold a second time to prevent charging of particles. For bulk analysis, half a filter was extracted in 2 ml of deionized water and analyzed for Na, SO_4, Ca, K, Mg, Fe, Si, Al, Zn and Ba using ICP-OES. Measured Na concentrations were a factor of 4–5 lower than expected on the basis of the elemental composition of ocean water. It should be noted that Na did not dissolve completely as polycarbonate filters are hygroscopic and can act as an ion exchange substrate.

Backward trajectories were calculated using the vertical motion model in the HYSPLIT4 (HYbrid Single-Particle Lagrangian Integrated Trajectory) program (Draxler and Rolph, 2003) with the FNL meteorological database at NOAA Air Resources Laboratory's web server (Rolph, 2003). Back trajectory calculations were started 10 m above ground level and several back trajectories were calculated for each sample every 2 h

ACPD
9, 3307–3365, 2009

during the 24 h sample collection period (Fig. 2). Trajectories were used together with meteorological parameters measured at Mace Head to classify air masses into 4 different groups, to which samples were assigned (Table 1).

3.2 Characterization of aerosol particles by automated SEM analysis

Prior to ion microprobe analysis, the samples were investigated by scanning electron microscopy (LEO 1530 FESEM) operating at an accelerating voltage of 10 keV, and equipped with an Oxford Instruments ultra-thin-window energy-dispersive x-ray (EDX) detector to characterize the chemical composition, size and shape of each individual grain. Filters were sampled at predefined equidistant spots. Whenever the predefined spots were located within a particle, the particle was counted and its size and chemical composition were measured. The 2-D surface area of each particle was measured by counting the number of pixels it occupied in the digital secondary electron image and converted to μm^2 (pixel size at 6000x=111 nm, pixel size at 18 000x=37 nm).Based on the 2-D surface area of the particle, the particle equivalent diameter was calculated. The equivalent diameter is the diameter of a spherical particle occupying the same area as the analyzed particle. Only particles with an area >100 pixels were considered for sizing to ensure accuracy of the estimated equivalent diameter (Gwaze et al., 2006). In order to retrieve the volume and mass of particles, the height of the particles needs to be ascertained. As the height of larger particles (typically shattered sea salt particles and sometimes dried droplets) is much less than the 2-D diameter, the height is estimated to be half the 2-D diameter for particles 1 µm<x<5 µm, based on manual analysis of numerous particles. The justification for taking these values is that particles in this size range typically consist of 1–3 sea salt crystals and the height is usually that of the individual units. The average height of particles >5 µm is considered to not exceed 2 µm, as large assemblies of shattered crystals and dried droplets (only a few nm in height) contributed to the particles in the larger size ranges. The approximate chemical composition of each particle is estimated on the basis of the analysis of seven energy windows in the EDX spectrum (N, Na, Mg, Si, S, Cl, and Ca for coarse mode

ACPD
9, 3307–3365, 2009

particles and Na, Si, S, Cl, K, Ca, and Fe for fine mode particles). The acquisition time was fixed at 2 s. Sampling regular spots is an established method to quantify the phase composition of samples with randomly distributed particles (Amelinckx et al., 1998). To avoid multiple sampling of the same particle, the distance between the spots has to be greater than the Feret's diameter of the largest particle. Whenever this criteria is fulfilled, the probability of acquiring an EDX spectrum of a particle of particular size and chemical composition is directly proportional to the total filter area covered with particles of that size and chemical composition and, therefore, to the number of the particles. This method allows fast quantification of the abundance of different particle types in the samples. The application of this method to the x-ray analysis of aerosol samples has several advantages:

1. The particle loading on the filter and the particle size distribution is estimated much more accurately than that based on image analysis alone, as long as a representative section of the filter is analyzed.

2. The EDX spectrum of the empty filter (background signal) depends on the geometry inside the instrument, i.e., the position of the filter with respect to the detector and the width of the energy window. For moderate particle loadings, the filter background signal can be estimated accurately for each sample and energy window separately using the upper (Q_u) and lower (Q_l) quartile values of the raw signals of that energy window by applying robust statistics as $Q_l - 1.726 \cdot (Q_u - Q_l) <$ filter background $< Q_u + 1.726 \cdot (Q_u - Q_l)$, which is equivalent to a 3σ outlier limit (Stoyan, 1998). The background signal is then subtracted from the particle signal.

3. Particles that lack contrast in the SEM image or are smaller than a predefined size cut-off are usually not accounted for by image based analysis methods. These particles can still be detected by their chemical signature. For calculating the aerosol mass they are considered to be smaller than the cut-off size.

ACPD
9, 3307–3365, 2009

Typically 500 particles of each sample were examined at two different magnifications: 18 000x (fine mode filter) and 6000x (coarse mode filter) for particles in the size ranges 0.4 µm–4 µm and 0.9 µm–20 µm, respectively. Chemical signals of particles below the detection limit of the image analysis (0.4 µm fine mode, 0.9 µm coarse mode) were found on both filters. After background correction, the x-ray intensities were normalized to the sum of intensities detected for the particle. The relative intensities for the major elements detected were used as a proxy for the particle composition. Particles were grouped based on their chemical composition and on the characteristics of different particle types observed in other studies (Xhoffer et al., 1991; Ebert et al., 2002; Li et al., 2003; Sobanska et al., 2003; Niemi et al., 2005). As the main objective of this research is the analysis of sulfur isotope ratios, particles that contained sulfate were treated separately (e.g., aged sea salt containing nitrates and mixed silicate/sea salt particles (Group 2) and aged sea salt containing nss-sulfate (Group2a), see Sect. 4.1.). Each particle chosen for sulfur isotope analysis was documented individually with a picture taken at higher magnification before and after analysis along with a full x-ray spectrum. Particles identified as ammonium sulfate based on the spectrum acquired during the automatic run were only documented after NanoSIMS analysis, because damage by the electron beam can alter their isotopic composition (Winterholler et al., 2008).

The bulk composition of the sample is calculated from single particle analysis by multiplying the mass of particles of each group (e.g., sea salt, aged sea salt, see Sect. 3.1.) in a given size interval by the average elemental composition of the respective particle group (Table 2). The elemental composition of group 2a (aged sea salt) and 8 (mixed sulfates) vary strongly from sample to sample, while other particle groups (e.g., sea salt) show only little variation. Therefore, for these two groups the average composition of each individual sample is used in the calculation.

3.3 Isotope analysis of individual particles with the Cameca NanoSIMS 50

The sulfur isotope measurements were done with the Cameca NanoSIMS 50 ion microprobe at the Max Planck Institute for Chemistry in Mainz (Hoppe et al., 2005; Hoppe,

ACPD
9, 3307–3365, 2009

2006; Gröner and Hoppe, 2006). This instrument is characterized by very good lateral resolution (<100 nm for Cs^+ primary ions), high transmission for secondary ions for isotope measurements of the light-to-intermediate-mass elements and multi-collection capabilities (up to 5 isotopes can be analyzed simultaneously).

The data in this study were obtained in multi-collection detector mode by sputtering the sample with a ~1 pA Cs^+ primary ion beam focused onto a spot of ~100 nm diameter. The primary ion beam was scanned over 2×2 μm^2 around the center of individual grains. Each analysis consisted of integration of secondary ion signals over 1200 cycles of 1 s each, preceded by 500 s or 200 s of pre-sputtering for coarse and fine mode samples, respectively. Coarse mode samples were coated with gold prior to ion microprobe analysis, and energy centering was used to compensate for charging. Secondary ions of $^{16}O^-$, $^{32}S^-$, $^{33}S^-$, $^{34}S^-$ and $^{36}S^-$ were simultaneously detected in five electron multipliers at high mass resolution. The detector dead time is 36 ns and the S^- count rates were corrected accordingly. Low-energy secondary ions were collected at a mass resolution sufficient to separate ^{33}S from the ^{32}SH interference. The energy slit was set at a bandpass of ~20 eV and the transmission was set at ~15–20% (specific setting of entrance, aperture, and energy slits). Here, we concentrate on the measured $^{34}S/^{32}S$ ratios because due to the low isotopic abundances of ^{33}S and ^{36}S the resulting errors of $^{33}S/^{32}S$ and $^{36}S/^{32}S$ ratios in single particles are large. The grain size and matrix dependence of the instrumental mass fractionation (IMF) were corrected based on the equivalent diameter and chemical composition measured for the respective particle in the SEM according to the method described in Winterholler et al. (2008). The necessity to correct for the size of the particles is caused by charging. Since the size determination of particles in the SEM is very accurate, this is a simple and straightforward correction, which is relevant mainly for coarse mode particles. Matrix dependent instrumental mass fractionation occurs during sputtering and ionization. Winterholler et al. (2008) found a linear relationship between the ionic radius of the cation (i.e., the chemistry) and the matrix specific instrumental mass fractionation for different sulfate salts. Riciputi et al. (1998) showed that the IMF of fine

ACPD
9, 3307–3365, 2009

grained mixed samples, which contain two phases on a spatial scale smaller than the primary ion beam, can be accurately corrected using coarse grained standards of the individual phases. The instrumental mass fractionation relative to $BaSO_4$ has been established for most sulfates relevant for atmospheric research (Winterholler et al., 2008). Correction of pure sulfate particles and "internally mixed" particles in which the sulfate containing phases are clearly separated such as the aged sea salt particle in Fig. 6 containing sodium sulfate on the surface of the sodium cloride cube and a gypsum needle as separat phases, is straightforward. This particle is a classical example of a particle that is "internally mixed" from an aerosol point of view, but "externally mixed", i.e., separated into distinct components on the spatial scale relevant for IMF correction in the NanoSIMS. IMF correction of particles contain several cations in the same sulfate (e.g. glauberite, $Na_2Ca(SO_4)_2$) is difficult. For such particles (part of the particles in group 6, mixed sulfates, <5% of the total particles) we calculated the IMF of the mixture based on the chemical composition of the respective particle as a linear mixture of the IMF of the pure salts of the major cations. The instrumental mass fractionation for each session was determined using two $BaSO_4$ standards (IAEA SO-5 and SO-6, Isotope Hydrology Laboratory of the International Atomic Energy Agency, Vienna, Austria). Individual particles of both standards were put on two gold coated Nuclepore filters with the help of a micromanipulator. Filters were then coated with gold a second time and analyzed along with the samples (Table 3, Fig. 3).

4 Results

4.1 Classification of particles by chemical composition

The approximate chemical composition of each particle was derived from the EDX spectra of seven energy windows (N, Na, Mg, Si, S, Cl, and Ca for coarse mode particles and Na, Si, S, Cl, K, Ca, and Fe for fine mode particles) and used to group particles into 11 groups. As oxygen was not analyzed, S was considered to be SO_4,

ACPD
9, 3307–3365, 2009

Si was considered to be SiO_2, and N was considered to be NO_3. Table 2 lists the semi-quantitative chemical composition for each group:

(1) *Sea salt* particles were recognized by high intensities of sodium and chlorine. Occasionally $MgCl_2$ and KCl particles were detected, but in general magnesium and potassium salts were found to be mixed with NaCl. Such chloride components crystallize in the atmosphere from seawater droplets (Fitzgerald, 1991). As sea salt contains sulfate (7.7% by mass), NaCl particles from sea salt can contain several percent of sulfate, even if their crystal structure is not suitable for accommodating it, in particular if the evaporation of droplets was too rapid to attain equilibrium during crystallization. Due to the high detection limit for sulfur in the EDX system, which is caused by the gold interference, no sulfur was detected in most NaCl particles during the automatic scans (2 s analysis). However, particles in which the sulfur content was below the detection limit of the EDX system still contain sufficient sulfur for NanoSIMS analysis. The sulfur content of such particles was estimated to be ~8.5%, based on the number of detected S atoms in the NanoSIMS. The product of transmission and ionization efficiency ($T*\varepsilon=2.7*10^4$) was calculated based on atomic force microscopy measurements of the material consumed during NanoSIMS analysis, the theoretical number of S atoms in the analyzed volume, and the number of detected S atoms for gypsum ($T*\varepsilon=3.1*10^4$), anhydrite ($T*\varepsilon=1.6*10^4$) and ammonium sulfate ($T*\varepsilon=3.4*10^4$).

(2) *Aged sea salt and mixed sea salt particles* were defined as sea salt particles that contain nitrates formed by the interaction of nitric acid with the alkaline sea salt particles (N>6%), or are mixed with quartz or other mineral dust particles (Si>6%, Ca>6% or Fe>6%).

(2a) *Aged sea salt particles containing sulfur*: Sea salt, aged sea salt or mixed sea salt particles for which sulfur has been detected in the EDX analysis were treated separately. Due to the high detection limit for sulfur in the EDX system, these particles typically contained >8.5% of sulfur and, therefore, significant amounts of nss-sulfate. Aged sea salt particles originate from the reaction of sea salt with atmospheric SO_2 and or H_2SO_4 giving rise to Cl depletion and sulfate formation (Zhuang et al., 1999). It

ACPD
9, 3307–3365, 2009

is generally observed that the amount of cations such as Mg, K and Ca increases with increasing sulfur content of the aerosol particles on a macroscopic and microscopic scale (Fig. 4, Table 2).

(3) *Quartz and silicates*: Particles with Si>90% were considered to be SiO_2 (quartz); particles with Si>6% with variable amounts of Na, Ca, K, Mg and Fe and without any Cl or S were considered to be alumosilicates. Silicon-bearing particles can be of natural origin (mineral dust, erosion of soil) as well as of anthropogenic origin (fly-ash). In both cases, they demonstrate continental influence on the air mass reaching Mace Head.

(3a) *Quartz and silicates with sulfur coating*: Almost all atmospheric particles can obtain a sulfur coating by in-cloud processing or condensation of SO_2 and/or H_2SO_4. Some alumosilicates, in particular alkali feldspars, might even react with sulfuric acid. All particles with Si>6% that do not contain Cl and have variable amounts of S have been put into this group.

(4) *Sodium nitrate* is formed by the reaction of nitric acid with the alkaline sea salt particles, causing Cl depletion in the process. When acid concentrations in the gas phase are high, this reaction can go to completion and pure $NaNO_3$ particles are formed (Na+N>90%)

(4a) *Sodium sulfate* is formed by the interaction of SO_2 and/or H_2SO_4 with NaCl particles. In strongly polluted air masses, entire particles can be converted to $NaSO_4/Na_2SO_4$, particularly in the fine mode.

(5) *Magnesium sulfate* is formed mainly by fractional crystallization of sea salt particles. Fractional crystallization can take place in the atmosphere or during sample collection. Rapid evaporation of sea water droplets leads to significant amounts of sea-salt-sulfate being trapped in NaCl crystals. Slow evaporation of seawater leads to the preferential formation of gypsum and magnesium sulfates (Borchert, 1965; Eugster et al., 1980; Zayani et al., 1999). After crystallization, sea salt particles can form loose aggregates that can shatter and produce pure crystals.

(6) *Sulfuric acid or ammonium (bi)sulfate*: S-only particles that show no association with other detectable elements (S>90%) were considered to be secondary sulfates

ACPD
9, 3307–3365, 2009

formed from gaseous SO_2. To confirm this, synthetic $(NH_4)_2SO_4$ grains in the size range of 0.5 µm–15 µm were spread on a gold coated Nuclepore polycarbonate filter, coated with gold like the aerosol samples, and analyzed with the same procedure as the aerosol samples. They showed no detectable elements other than S, when the energy windows N, Na, Mg, Si, Cl, S and Ca were chosen for the analysis. Unfortunately, gold interferes with sulfur in the EDX spectrum, making high background correction necessary. Small S-only particles were therefore missed by single particle analysis. This missing fine mode ammonium sulfate was quantified by bulk analysis of the aerosol samples.

(7) $CaSO_4$ *particles* were identified by the absence of all elements other than Ca and S. The most abundant minerals are gypsum and anhydrite. Primary gypsum particles have natural (soil, mineral dust, fractional crystallization of sea salt) as well as anthropogenic sources (flue gas desulfurization, metal and cement industry, and road dust) (Hoornaert et al., 1996; Li et al., 2003). Reactions between sulfuric acid and $CaCO_3$ or Ca-feldspars can result in the formation of secondary gypsum (Foner and Ganor, 1992). Marine sources of $CaCO_3$ include fractional crystallization of sea water and biogenic particles, e.g., coccoliths (Andreae et al., 1986).

(8) *Mixed sulfates*: All particles containing sulfur that could not be grouped into any of the above groups are referred to as mixed sulfates. These include sulfate particles formed during fractional crystallization of sea salt with more than one cation, potassium sulfate and large S-only particles (>2 µm), which derive from in-cloud processing rather than condensation of sulfuric acid. Sulfide minerals (FeS_2) were absent in all samples.

(9) *Calcite and Dolomite*, $CaCO_3$ and $CaMg(CO_3)_2$, are characterized by a relative intensities of Ca or Ca+Mg higher than 90%. The sources of these particles are soil erosion and industrial activities such as stone dressing, cement and metal industries (Hoornaert et al., 2003).

(10) *Iron oxides or hydroxides*: Particles containing Fe>90% but no Cl, Si or S are considered to be oxides (hematite, magnetite) or hydroxides (goethite), all of which are soil minerals.

(11) *Not classified*: All particles that could not be classified into any of the above mentioned groups. These are mainly carbonaceous particles with traces of Na and K, particles with several cations but no detected anion, or particles for which only one element was above the detection limit. The latter are most frequently found in the smallest particles size range (<400 nm).

Typical micrographs and EDX spectra of individual particles of each group (except groups 4 and 9) are shown in Fig. 5, and the contribution of each group to the total aerosol number is shown in Table 4.

The most abundant particle group for all samples was sea salt (NaCl) which accounts for more than 50% of total particle number (Table 4) in all samples, except the fine mode of samples 5, 6 and 8. Based on the aerosol composition, samples were divided into two classes. The first class ("clean") was dominated by sea salt, aged sea salt and ammonium sulfate with no or moderate chlorine depletion (samples 1, 2, 3, 4, 9, 10, 11, 12, 14 and 16). The second class of samples ("polluted") showed significant chlorine depletion, particularly for fine mode particles (samples 5, 6 and 8). The fine mode sea salt particles had been almost completely converted to sulfates. Sodium sulfate, sodium nitrate and ammoniums sulfate particles dominate the fine mode aerosol and sodium nitrate particles are present in the coarse mode of polluted samples. In the "clean" samples, sea salt typically accounted for >60% of both fine mode and coarse mode particle number, and Na+Cl represented approximantely 85% of the total particle mass (calculated from Table 5). Four of these samples (Sample 3, 4, 10 and 16)) showed high numbers of ammonium sulfate/sulfuric acid particles in the fine mode (>18%). Samples 9, 10, 11, 12, 14, and 16 had the highest concentrations (>15%) of coarse mode aged sea salt particles. Finally, samples 5, 6 and 10 were characterized by very low fine mode particle mass <400 ng/m^3 (Table 5).

4.2 Isotopic composition of different types of sulfate aerosol

Chemical analysis of Mace Head aerosol identified eight groups of sulfate-containing particles. The contribution of each of these groups to the sulfate content of each sam-

ACPD
9, 3307–3365, 2009

ple was calculated based on results from single particle and bulk analysis (Table 6). The isotopic composition of each group was measured by NanoSIMS (Fig. 6, Table 6). Details of all analyses are provided in an online supplement.

Sea salt (Group 1) particles contained only sea-salt-sulfate and little or no nss-sulfate. Still, enough S was present to allow analysis by NanoSIMS. The isotopic composition of sulfur in Sea salt sulfate in NaCl particles was on average δ^{34}S=(20.6±1.3)‰Ėarlier measurements of gypsum particles formed during fractional crystallization of sea salt indicated an isotopic composition of (23±1)‰ (Winterholler et al., 2006). The data reported here agree well with the isotopic composition of seawater (δ^{34}S=20.7‰), with Rayleigh fractionation occurring during fractional crystallization of sea salt particles (Raab and Spiro, 1991). NaCl particles from sea salt typically contributed 40–55% to the total sulfate of "clean" samples and 10–20% to the total sulfate of "polluted" samples.

Ammonium sulfate/sulfuric acid or mixed organic/sulfuric acid (Group 6) particles typically contributed 15–35% of total sulfate under "clean" conditions and 30–65% under "polluted" conditions and comprised a significant portion of the fine mode aerosol. Analysis of ammonium sulfate/sulfuric acid particles failed frequently, as the small size of these particles coupled with the high sputter rate of >2 nm/s in this material did not permit successful analysis. For samples in which such particles could not be measured, this is a source of major uncertainty in calculating the bulk isotopic composition, as well as in estimating the isotopic composition of the source SO_2. The isotopic composition of ammonium sulfate measured in "clean" samples ranged from δ^{34}S=(−9±4)‰ to (+5±3)‰. (Table 6).

Aged sea salt particles typically contained 19% of sulfur under "clean" conditions and 29% under "polluted" conditions (Group 2a, Table 2). The contribution to the total sulfate of the individual sample ranged from 5–30% for both "clean" and "polluted" samples. The isotopic composition of aged sea salt particles of "clean" samples was between δ^{34}S=(3±3)‰ and (20±2)‰ (Table 6). "Polluted" samples showed an average isotopic composition of δ^{34}S=(14±4)‰.

ACPD
9, 3307–3365, 2009

Sodium sulfate (Group 4a) presents the final step in the chlorine depletion of sea salt (see Sect. 4.1). Its contribution to aerosol sulfate under "clean" conditions was minor (typically 0–4%), while under "polluted" conditions it contributed ~10%. The isotopic composition could only be measured for "polluted" samples and was on average δ^{34}S=(6±5)‰.

Mixed sulfates (Group 8) contributed 0–15% to "clean" and 5–10% to "polluted" samples. The measured isotopic composition for mixed sulfates in "clean" samples ranged from δ^{34}S=(4±5)‰ to (12±4)‰For "polluted" samples the isotopic composition was on average δ^{34}S=(8±3)‰ (Table 6).

The contribution of silicates with sulfur coating (Group 3a) to total sulfate was only minor (<3%). The sulfur in these particles is derived mainly from the condensation of sulfuric acid. However, heterogeneous oxidation of sulfur might occur on mineral dust containing Fe(III) or Mn(II). The isotopic composition of sulfur coatings on silicates was measured for "clean" samples (δ^{34}S=(6±6)‰) only. The only particle analyzed from a "polluted" sample was found to be coated with aged sea salt upon closer inspection (δ^{34}S=(11±6)‰).

Magnesium sulfate (Group 5) and gypsum (Group 7) typically contributed only 0–5% to total aerosol sulfates. The isotopic composition of magnesium sulfate was measured only for two "clean" samples (δ^{34}S=(23±7)‰ samples 1 and 4).

The isotopic composition of gypsum was analyzed for one "clean" (δ^{34}S=(14±7)‰ sample 1) and one "polluted" sample (δ^{34}S=(19±6)‰ sample 8).

The bulk isotopic composition of each sample was calculated based on the isotopic composition of each group and the fraction that it contributed to the total sulfate:

$$\delta^{34}S_{bulk} = \sum f_i \cdot \delta^{34}S_i \quad (2)$$

and the error of the calculated bulk composition is

$$\sigma_{bulk} = \sqrt{\left(\sum (f_i \cdot \sigma_i)^2\right)} . \quad (3)$$

ACPD
9, 3307–3365, 2009

Missing measurements on sea salt particles were replaced by the isotopic composition of sea water (δ^{34}S=(20.7±0.3)‰), missing values for ammonium sulfate/sulfuric acid particles by the isotopic composition of nss-sulfate formed by homogeneous oxidation estimated from aged sea salt particles (Table 7, see Sect. 4.4), and all other missing values (e.g. sodium sulfate sample 1) were taken as (0±20)‰. The bulk isotopic composition of "clean" samples ranged from $\delta^{34}S_{bulk}$=(8±2)‰ to (15±3)‰. The bulk isotopic composition of "polluted" samples is $\delta^{34}S_{bulk}$=(7±2)‰ (sample 6) and δ^{34}S=(1±2)‰ (sample 8).

4.3 Non-sea-salt-sulfate content of different particle types

As the objective of this work is to understand the formation process of secondary sulfate aerosol, the influence of primary sulfate on the measured isotopic composition has to be accounted for. The dominant primary sulfate at Mace Head is sea-salt-sulfate (δ^{34}S=+20.7‰). In order to estimate the sulfur isotopic composition of the nss-sulfate in different types of aerosol particles such as aged sea salt, sodium sulfate, magnesium sulfate, gypsum, mixed sulfates and ammonium sulfate/sulfuric acid particles, the sea-salt-sulfate content of these particle groups has to be estimated. Then sea-salt-sulfate is subtracted from the isotope signature of the respective particles to calculate the nss-sulfate isotopic signature

$$\delta^{34}S_{particle,nsss}=\delta^{34}S_{particle}-f_{seasalt}\cdot+0.0207 \quad (4)$$

Ammonium sulfate/sulfuric acid particles (Group 6) do not contain any sea-salt-sulfate and NaCl particles from the sea salt (Group 1) do not contain any non-sea-salt-sulfate. The sea-salt-sulfate content ($f_{seasalt}$) in aged sea salt (Group 2a), sodium sulfate (Group 4a) and mixed sulfate (Group 8) particles was calculated based on the average sodium and sulfur content of these particle groups for each individual sample as derived from single particle analyses. For "clean" samples the sulfur content of aged sea salt particles had to be estimated based on the number of detected sulfur ions and

ACPD
9, 3307–3365, 2009

the material consumed during NanoSIMS analysis.

$$\text{Sea-salt-sulfate} = [\text{Na}] \cdot 0.252 \quad (5)$$

$$\text{Non-sea-salt-sulfate} = [\text{SO}_4] - [\text{Na}] \cdot 0.252 \quad \text{(Krouse and Grinenko, 1991)} \quad (6)$$

The nss-sulfate content of gypsum (Group 7) and magnesium sulfate (Group 5) is difficult to estimate. Due to the preferential formation of these phases during fractional crystallization of sea salt (see Sect. 4.1), pure gypsum and magnesium sulfate particles are formed. This does not enrich these phases in non-sea-salt-sulfate with respect to the droplet from which the precipitation of these phases occurred. The average nss-sulfate fraction of the bulk sample is considered to be representative of the average composition of the droplets. It was, therefore, assumed to be valid for both groups.

4.4 Isotopic composition of source SO_2

The isotopic composition of the nss-sulfate depends on two factors, the isotopic composition of the source SO_2, and the oxidation process responsible for the formation of nss-sulfate. In order to interpret the measured data one of these two factors needs to be eliminated, i.e., for interpreting sulfur isotope data of secondary sulfate in terms of the source composition of the SO_2, the oxidation process needs to be known, and to understand the oxidation process the source composition has to be identified first.

As described earlier, fine mode ammonium sulfate is used as a proxy for the isotopic composition of nss-sulfate formed by the homogeneous oxidation pathway (Table 6, Fig. 7, 0% sea-salt-sulfate, 100% homogeneous oxidation, grey square). In cases, where no fine mode ammonium sulfate was successfully analyzed, sulfate coatings on silicates are the next best proxy used (Table 6, Fig. 7, 0% sea-salt-sulfate, 100% homogeneous oxidation, open square). For samples in which neither of the two is available, the isotopic composition nss-sulfate from homogeneous oxidation has to be estimated based on the single particle nss-sulfate data of the respective samples. Typically the isotopic composition of nss-sulfate in aged sea salt, sodium sulfate and mixed sulfates shows:

ACPD
9, 3307–3365, 2009

1. Numerous particles with an isotopic composition corresponding to the homogeneous oxidation pathway.

2. A tail towards higher values, that is due to a mix of both oxidation pathways, contribution to the nss-sulfate in the same particles and

3. Few particles containing nss-sulfate formed by heterogeneous oxidation only.

The two modes corresponding to the homogeneous and heterogeneous oxidation lie ~(28±2)‰ apart at 0% sea-salt-sulfate (Table 7, Fig. 7). Within analytical error this agrees with the expected difference of ~25.5‰ (Tanaka et al., 1994). Therefore, the isotopic composition of nss-sulfate in aged sea salt, sodium sulfate and mixed sulfates can be used to estimate the isotopic composition of the source SO_2 ($\delta^{34}S_{SO_2}=\delta^{34}S_{hom.\ oxidation}+0.009=\delta^{34}S_{het.\ oxidation}-0.0165$‰; cf. Sect. 2).

The isotopic composition of source SO_2 is $\delta^{34}S$=(14±3)‰ (13±5)‰ and (11±6)‰ for samples 1, 2 and 3, respectively. These three samples display a strong marine biogenic contribution to source SO_2 and are plotted in Fig. 7a.

Samples 4, 9, 10, 11 and 16 were classified as "clean" samples based on chemical composition, but the isotopic signature of the source SO_2 ($\delta^{34}S$=(0±4)‰ (8±3)‰, (5±6)‰, (0±3)‰ and (3±2)‰, respectively) indicates that nss-sulfate in these samples derives mainly from the oxidation of SO_2 from anthropogenic pollution. "Clean" samples with an anthropogenic signature of source SO_2 are shown in Fig. 7b. Sample 4 presents a more complex case. A pollution event occurred towards the end of the sampling period. Therefore, different source SO_2 contributed to the formation of different particles types in the same sample. Therefore, the isotopic composition of source SO_2 estimated by different methods differs more than it is observed for all other samples. Ammonium sulfate particles were formed predominantly during the pollution event and indicated an anthropogenic signature for the source SO_2 ($\delta^{34}S_{SO_2}$=(0±4)‰). Aged sea salt, magnesium sulfate and mixed sulfate particle derived mainly from the period before the pollution event. If the second mode of aged sea salt, magnesium

ACPD
9, 3307–3365, 2009

sulfate and mixed sulfate particles ($\delta^{34}S_{SO_2}=\delta^{34}S_{het.\ oxidation}-0.0165‰$) is used for estimating the source SO_2, results indicate a predominantly biogenic origin of source SO_2 ($\delta^{34}S_{SO_2}=(11\pm7)‰$). Therefore, in this sample nss-sulfate in ammonium sulfate particles is considered to be of predominantly anthropogenic origin, while nss-sulfate in other particle types is considered to be of marine biogenic origin.

"Polluted" samples (samples 6 and 8) with an anthropogenic signature of source SO_2 are shown in Fig. 7c and show an isotopic composition of $\delta^{34}S_{SO_2}=(3\pm1)‰$ and $(3\pm2)‰$, respectively.

4.5 Contribution of homogeneous and heterogeneous oxidation to nss-sulfate formation in different types of aerosol particles

Figure 7 demonstrates how the contribution of heterogeneous oxidation to nss-sulfate was calculated. It shows the isotopic composition of all the individual particle groups (1, 2a, 3a, 4a, 5, 6, 7 and 8) and bulk samples plotted against the sea-salt-sulfate content of the respective particle type/sample (see Sect. 4.3) for each sample. This allows separation of the influence that variable amounts of primary sea-salt-sulfate have on $\delta^{34}S$ (mixture of primary and secondary sulfate) from the isotope fractionation effect during oxidation. The effect of variable source SO_2 is eliminated by plotting samples with different source SO_2 separately. "Clean" samples with a significant contribution of marine biogenic source SO_2 to nss-sulfate (see Sect. 4.4) are shown in Fig. 7a (samples 1, 2 and 3, $\delta^{34}S_{SO_2}=\sim12‰$), "clean" samples with nss-sulfate deriving from oxidation of anthropogenic source SO_2 in Fig. 7b (samples 4, 9, 10, 11 and 16, $\delta^{34}S_{SO_2}=\sim3‰$), and "polluted" samples in Fig. 7c (samples 6 and 8, $\delta^{34}S_{SO_2}=\sim3‰$). The average isotopic composition of the source SO_2 of the samples plotted in each panel is given on the upper right hand corner of the panel. The isotopic composition of all the particles analyzed of each particle group, in each sample, was averaged to decrease the uncertainty of the measured isotopic composition. The error of sulfur isotope analyses of individual particles by NanoSIMS is typically ~5‰ due to inherent limitation in the

ACPD
9, 3307–3365, 2009

reproducibility caused by the morphology of the grains (Winterholler et al., 2008). The reproducibility of repeated measurements on the same particle is typically <2‰, even if analyses are performed in separate sessions. Therefore, averaging over several grains increases the accuracy of the analysis significantly. All values presented in Fig. 7 are listed in Table 6, except for aged seas salt, sodium sulfate and mixed sulfates where coarse and fine mode were plotted separately in Fig. 7. The standard error σ as given in Table 6 includes the high standard deviation of the isotopic composition caused by the presence of both oxidation pathways in separate particles within the same particle group (i.e., the error of the weighted mean is multiplied by sqrt(χ^2) for χ^2>1) and, therefore, includes the natural variability of the sample. In Fig. 7 error bars give the 1σ error of the weighted mean (i.e., the analytical error only).

The average isotopic composition of sea-salt-sulfate (x=100) and nss-sulfate produced by homogeneous oxidation of SO_2 (x=0, intercept of the solid line) are estimated from a line fit (solid line) to all data points of Group 1 (sea-salt-sulfate only), Group 3a and 6 (100% homogeneous oxidation). Both values are given in the upper right corner of each panel. Whenever the isotopic composition of a particle group is dominated by condensation of H_2SO_4(g) onto sea salt aerosol, values are expected to lie on this regression line. The contribution of heterogeneous oxidation to the sample produces a tendency towards higher isotopic signatures. The isotopic composition of 0% sea-salt-sulfate and 100% heterogeneous oxidation is expected to be ~+25.5‰ with respect to 0% sea-salt-sulfate 100% homogeneous oxidation. The upper limit expected for particles containing nss-sulfate formed by heterogeneous oxidation only is indicated by the dashed line.

The contribution of heterogeneous oxidation to a given particle group is equivalent the vertical distance of its isotopic composition to the mixing line between nss-sulfate derived from homogeneous oxidation and sea-salt-sulfate and the mixing line between nsss-sulfate derived from heterogeneous oxidation and sea-salt-sulfate . For example, the mixing line fit for Panel a is y=(21±2)·x+(3±1)‰ giving an isotopic composition of δ^{34}S=(24±3)‰ to the sea-salt-sulfate, and an isotopic composition of δ^{34}S=(3±1)‰ to

ACPD
9, 3307–3365, 2009

nss-sulfate derived from homogeneous oxidation. The contribution of heterogeneous oxidation is illustrated using the coarse mode aged sea salt of sample 3 (open circle) at 20% sea-salt-sulfate (f_{sss}=0.2) and δ^{34}S=(23±4)‰ ($\delta^{34}S_{nsss}$=(19±4)‰). The contribution of heterogeneous oxidation in % is calculated as

$$f_{i,het} = (\delta^{34}S_{i,nsss} - \delta^{34}S_{hom})/(0.0257 \cdot (1 + \delta^{34}S_{hom})) \quad (7)$$

and the error as

$$\sqrt{(\sigma^2_{i,nsss} + \sigma^2_{hom})}/(0.0257 \cdot (1 + \delta^{34}S_{hom})). \quad (8)$$

i.e., f_{het}=(0.019−0.003)/(0.0257·1.003)=0.62±0.16.

The fraction of heterogeneous and homogeneous oxidation pathway calculated by this equation is very sensitive to the isotope fractionation assumed for both pathways and any change in these constants due to fresh experimental evidence would affect the calculations. However, the fractionation constant of gas phase oxidation (α_{hom}=0.991, Tanaka et al. 1994) is used to calculate $\delta^{34}S_{SO_2}$ based on the isotopic composition of ammonium sulfate particles. The results are in agreement with the air-mass history and current knowledge about marine isotope chemistry of sulfate. We, therefore, believe that the calculations by Tanaka et al. provide an accurate estimate of the fractionation factor. The line fits for Panels b and c are y=(27±2)·x−(6±1)‰ and y=(28.5±0.9)·x−(6.5±0.5)‰ respectively. For polluted samples, measurements of ammonium sulfate were missing, as all analyses on the fine mode filter failed. Therefore, the isotopic composition of nss-sulfate produced by heterogeneous oxidation, which is needed for the line fit, was estimated from the nss-sulfate isotopic composition of aged sea salt (Fig. 7c, marked by a cross). This corresponds to a $\delta^{34}S_{SO_2}$=~3‰ consistent with the value found for anthropogenic SO_2 in the "clean" samples shown in Fig. 7b.

The contribution of heterogeneous oxidation to the secondary sulfate in bulk samples is based on the contribution of heterogeneous oxidation to the individual group such as

ACPD
9, 3307–3365, 2009

aged sea salt, and the fraction that each group contributed to the total nss-sulfate:

$$f_{secondary,het} = \sum (f_{secondary,i} \cdot f_{i,het}). \quad (9)$$

and the error of the estimate is

$$\sum_{secondary,het} = \sqrt{[\sum (f_{i,secondary} \cdot \sigma_{fi,het})^2} \quad (10)$$

As Group 6 (ammonium sulfate/sulfuric acid particles) derived from homogeneous oxidation only, $f_{6,het}$ is 0 by definition. Group 1 does not contain any non sea-salt-sulfate. Therefore, $f_{1,nsss}$ is 0.

Figure 7a presents "clean" samples for which marine biogenic sources contributed significantly to nss-sulfate. For these samples the contribution of heterogeneous oxidation to nss-sulfate in coarse mode aged sea salt (f_{het}=−0.04±0.06) and mixed sulfate particles (f_{het}=−0.18±0.14) was negligible for samples 1 and 2, and significant only for coarse mode aged sea salt particles of sample 3 (f_{het}=0.62±0.16). The contribution of heterogeneous oxidation to nss-sulfate formation in fine mode aged sea salt (f_{het}=0.27±0.06) and mixed sulfate particles (f_{het}=0.64±0.17) was significant. For gypsum (f_{het}=0.04±0.27) and magnesium sulfate (f_{het}=0.39±0.27), the number of analyzed particles was too low to get a reliable estimate of the contribution of heterogeneous oxidation, based on the particles shown in Fig. 7a. The contribution of heterogeneous oxidation to bulk samples is negligible for all samples.

Figure 7b depicts "clean" samples for which anthropogenic sources dominated the nss-sulfate (samples 4, 9, 10, 11 and 16). One of the samples, sample 4, shows two outliers (fine mode aged sea salt and magnesium sulfate) and presents a more complex case (see Sect. 4.4). This sample is shown in Panel b, as the isotopic signature of ammonium sulfate particles determines the line fit and dominates the nss-sulfate of the bulk samples. Nevertheless, those aged sea salt, magnesium sulfate and mixed sulfate particles to which heterogeneous oxidation contributed seem to be formed predominantly from marine biogenic SO_2 during the first part of the sampling

ACPD
9, 3307–3365, 2009

period. Therefore, estimates for the contribution of heterogeneous oxidation to the formation of these particles in sample 4 are calculated using the line fit of Panel 7a.

For samples depicted in Panel b, the contribution of heterogeneous oxidation to the formation of nss-sulfate in coarse mode particles is negligible for aged sea salt particles (f_{het}=0.02±0.05) in all but one sample (sample 16: f_{het}=0.46±0.08), low for mixed sulfate particles (f_{het}=0.19±0.09) and significant only for magnesium sulfate particles (f_{het}=0.48±0.20). The contribution of heterogeneous oxidation to nss-sulfate formation in fine mode particles is negligible for aged sea salt particles of samples 10 and 16 and mixed sulfate particles of sample 16 (f_{het}=−0.06±0.9), but high in aged sea salt particles in sample 4 (f_{het}=0.62±0.12). The contribution of heterogeneous oxidation to bulk nss-sulfate is negligible for all these samples.

Figure 7c depicts "polluted" samples (6 and 8) with predominantly anthropogenic source SO_2. The contribution of heterogeneous oxidation to the formation of nss-sulfate is negligible only for the coarse mode sodium sulfate in sample 6 (f_{het}=0.13±0.12) and high for all other coarse mode particles (coarse mode aged sea salt: f_{het}=0.63±0.05; coarse mode sodium sulfate in sample 8: f_{het}=0.49±0.18; coarse mode mixed sulfates: f_{het}=0.66±0.08; coarse mode gypsum: f_{het}=0.87±0.24 and fine mode sodium sulfate (f_{het}=0.76±0.19). Due to the high contribution of ammonium sulfate particles to nss-sulfate, no significant contribution of heterogeneous oxidation to any of the bulk samples has been observed.

4.6 Comparison of chemical and isotopic composition in different air masses

From 30 September to 2nd October 2005 (samples 1 and 2), air masses from a high pressure region over Greenland descended slowly towards Mace Head and had only a short residence time in the marine boundary layer (MBL, Fig. 2a). Final transport in the MBL was rapid and local wind speeds were high. Relative humidity of the air masses was comparatively low and the local wind direction was N-NNW. The chemical composition of these samples (samples 1 and 2, Table 4) was dominated by sea salt particles. Aerosol sulfate (Table 6) was dominated by sea-salt-sulfate (>40%) and am-

monium sulfate (~30%), with ammonium sulfate being the dominant nss-sulfate component (60%–80% of nss-sulfate). The contribution of aged sea salt to total sulfate and nss-sulfate was low (5–10%). The isotopic composition measured on ammonium sulfate (δ^{34}S=+(5±3)‰ sample 1, δ^{34}S=(1±7)‰ sample 2) and sulfuric acid coating of a quartz particle (δ^{34}S=(6±6)‰) indicated an isotopic composition of the source SO_2 (δ^{34}S=(14±3)‰ and (13±5)‰) that implies a high contribution of biogenic sources to the nss-sulfate in these two samples. Taking an average isotopic composition of anthropogenic SO_2 at Mace Head of δ^{34}S=(3±1)‰ (Table 7), and δ^{34}S=(17.4±0.7)‰ for nss-sulfate from the oxidation of DMS (Sanusi et al., 2006), the contribution of marine biogenic sources is $f_{biogenic}$=0.76±0.21 for sample 1 and 0.69±0.35 for sample 2. The contribution of heterogeneous oxidation to the total nss-sulfate in both samples was minor due to the high ammonium sulfate content of both samples. On the other hand, the contribution of heterogeneous oxidation to fine-mode aged sea salt (f_{het}=0.27±0.06) and fine-mode mixed sulfates (f_{het}=0.64±0.17) was high.

From 3 and 4 October (samples 3 and 4), westerlies transported air masses from the east coast of Canada to Mace Head (Fig. 2b). Local winds shifted from the west on 3 October to the south on 4 October. Wind speeds were low and relative humidity was around 80%. Total sulfate in these samples was dominated by sea-salt-sulfate in sodium chloride particles (~40%) and by ammonium sulfate (~35%). The contribution of aged sea salt to total sulfur was higher than that of samples 1 and 2 (10–25%), while that of sea salt and ammonium sulfate was slightly lower. The isotopic composition of ammonium sulfate could only be measured for sample 4 (coarse filter δ^{34}S=(−9±6)‰ fine filter δ^{34}S=(−9±7)‰). Particles on sample 3 were too small for successful analysis. The isotopic composition of the source SO_2 was estimated as δ^{34}S=(11±6)‰ for sample 3, δ^{34}S=(11±6)‰ for nss-sulfate in aged sea salt, mixed sulfate and magnesium sulfate particles in sample 4 and δ^{34}S=(0±4)‰ for ammonium sulfate particles in sample 4. The contribution of heterogeneous oxidation to the bulk nss-sulfate was negligible for all samples. Nevertheless, heterogeneous oxidation contributed significantly to nss-sulfate in coarse mode aged sea salt of sample 3 (f_{het}=0.62±0.16) and fine

ACPD
9, 3307–3365, 2009

mode aged sea salt of sample 4 (f_{het}=0.62±0.12). The contribution of marine biogenic sources to nss-sulfate was $f_{biogenic}$=0.56±0.42 for sample 3 and $f_{biogenic}$=−0.21±0.28 for sample 4.

From 5 to 7 October (samples 5, 6 and 8), overcast but dry conditions and easterly winds brought polluted air to Mace Head (Fig. 2c). Relative humidity was typically 80–90%. In these samples, fine-mode sea salt was converted to sulfate, coarse modes samples contained less sea salt particles (<60%), and most sea salt particles showed traces of reactions with sulfate and nitrate. Total sulfate was dominated by ammonium sulfate (30–65%), sea-salt-sulfate in sodium chloride particles (10–20%), aged sea salt (5–25%) and sodium sulfate particles (~10%). The average isotopic composition of aged sea salt (δ^{34}S=(14±4)‰), sodium sulfate (δ^{34}S=(6±5)‰) and that of mixed sulfates (δ^{34}S=(8±3)‰) agreed within errors. The isotopic composition of source SO_2 was estimated as δ^{34}S=(3±1)‰ which agrees well with a predominately anthropogenic origin of nss-sulfate in these samples (f_{anth}=1.00±0.06). The contribution of heterogeneous oxidation to nss-sulfate aerosol is difficult to estimate as only few fine mode particles have been analyzed successfully, resulting in a high error of the estimate (Table 6). Heterogeneous oxidation contributed to coarse mode aged sea salt (f_{het}=0.63±0.05), mixed sulfates (f_{het}=0.66±0.08) coarse mode sodium sulfate (f_{het}=0.49±0.18) and fine mode sodium sulfate (f_{het}=0.76±0.19).

From 25 to 30 of October (samples 9, 10, 11, 12, 14 and 16), several frontal systems tracked over Mace Head that delivered significant precipitation on most days (Fig. 2d). Wind direction changed from westerly on 25 and 28 October to southerly on 26–27 October and 29–31 October. Relative humidity ranged typically from 70 to 100%. The chemical composition of the aerosol in this period is characterized by high numbers of aged sea salt particles accounting for >20% of total particulate sulfate. In this period, many particles were not dried completely by the drier during sample collection and were surrounded by a droplet (Fig. 8). In the region outlined by the droplet, the filter substrate was damaged, probably due to high acid content. The isotopic composition of aged sea salt for all analyzed samples ranged from δ^{34}S=(3±3)‰ on 27–28 Octo-

ACPD
9, 3307–3365, 2009

ber to ~(8±2)‰ on 26–27 October and 30–31 October. The isotopic composition of ammonium sulfate could be measured only for sample 10 (26–27 October, (−4±6)‰), suggesting an isotopic composition of (5±6)‰ for the source SO_2 in the air masses reaching Mace Head from a southerly direction. The isotopic composition of the source SO_2 for samples 9, 11, 16 was estimated from aged sea salt particles (^{34}S=(8±3)‰ (0±3)‰ and (3±2)‰, respectively). The average contribution of anthropogenic sulfur to nss-sulfate is f_{anth}=0.96±0.11. There was no significant contribution of heterogeneous oxidation to total nss-sulfate formation. It contributed only to the coarse mode aged sea salt of sample 16 (f_{het}=0.46±0.09) and mixed sulfates (f_{het}=0.19±0.09).

5 Discussion

The overall isotopic composition of the aerosol samples investigated in this study, deduced from single particle measurements, agrees well with previous studies of the bulk sulfur isotopic composition of aerosol at Mace Head (McArdle and Liss, 1995; McArdle et al., 1998). The analysis of McArdle and Liss (1995) yielded values of $\delta^{34}S$=(5±0.7)‰ at 0% sea-salt-sulfate and (19.7±3.6)‰ at 100% sea-salt-sulfate. Our data gives $\delta^{34}S$=(−3.3±1.2)‰ at 0% sea-salt-sulfate and (21.9±4.0)‰ at 100% sea-salt-sulfate, when Fig. 7a–c are combined. The intercept of our data is slightly lower than that published by McArdle and Liss (1995). This might reflect a change in the source signature of anthropogenic emission during the 10 year period between the two studies. Such changes can be caused the introduction of flue gas desulfurisation technology, as flue gas desulfurization enriches ^{34}S in the products and depletes the remaining SO_2 (Sinha et al., 2008; Derda and Chmielewski, 2003), as well as by the use of imported coal and changes in the suppliers of ship crude. The isotopic composition of anthropogenic SO_2 reaching Mace Head from the British Islands (samples 6 and 8, $\delta^{34}S$=~(3±1)‰), agrees well with the average isotopic composition of anthropogenic pollution over the British Islands in 2000 ($\delta^{34}S$=2‰), as estimated by Zhao et al. (2003).

ACPD
9, 3307–3365, 2009

During our sampling period, the average nss-sulfate loading was 0.5 µg/m^3 and the average contribution of marine biogenic sulfur was ~14%. Previous research found an average of 0.4–0.6 µg/m^3 nss-sulfate and ~3% marine biogenic sulfur for the month of October in 1988–1991 (Savoie et al., 2002).

Sulfate aerosol in our samples is mainly in the form of sea-salt-sulfate (10–60%) and ammonium sulfate/sulfuric acid particles (15–65%). Our results suggest that a significant portion of nss-sulfate in coastal regions is converted to fine mode ammonium sulfate (40–80%), and that condensation of H_2SO_4(g) contributes significantly even to the nss-sulfate in aged sea salt particles (20–100%). Modeled data (Barrie et al., 2001) suggest the existence of additional pathways of SO_2 oxidation in the outflow region of European and American pollution over the Atlantic. Previous research at Mace Head supported an additional pathway for gas phase oxidation of SO_2 (Berresheim et al., 2002), which is in agreement with our results. This additional oxidation pathway seems to involve kinetic fractionation similar to, or slightly stronger than that proposed for the oxidation by OH (Tanaka et al., 1994), as the difference in the isotopic composition observed for the gas-phase and heterogeneous oxidation pathway in our dataset is (28±2)‰.

The contribution of heterogeneous oxidation to nss-sulfate formation on aged sea salt sodium sulfate, magnesium sulfate gypsum and mixed sulfate particles under clean conditions is on average 10% for coarse and 25% for fine mode particles. The contribution of heterogeneous oxidation to nss-sulfate formation on aged sea salt sodium sulfate, magnesium sulfate gypsum and mixed sulfate particles under polluted conditions is on average 58% on coarse and 75% on fine mode particles. Alexander et al. (2005) estimated heterogeneous oxidation by ozone during the INDOEX cruise and found a higher contribution of heterogeneous oxidation to coarse mode samples compared to fine mode samples, which is in agreement with our results, if the large contribution of ammonium sulfate to our fine mode samples is considered. However, if only sea salt particles are taken into account, our dataset shows that heterogeneous oxidation is a more efficient process in fine mode sea salt particles compared to coarse mode

sea salt particles, which indicates that the heterogeneous oxidation is a surface limited process (the surface to mass ratio is more favorable in smaller particles). The absolute contribution of heterogeneous oxidation to nss-sulfate formation in bulk samples is lower (~5% under "clean" and ~20% under "polluted" conditions) than the 10–30% contribution of heterogeneous oxidation via O_3 reported by Alexander et al. (2005) for the Indian Ocean. Overall, the contribution of heterogeneous oxidation calculated based on sulfur isotope analysis of particles in Mace Head is much lower than the global annual average contribution of heterogeneous processes to sulfur oxidation of 84% (Alexander et al., 2008): This again might point toward a high contribution of rapid gas phase oxidation in coastal regions of the northern latitudes compared to the open ocean. Recent application of the same technique to urban air samples found a range of 40–100% heterogeneous oxidation for different days in August 2005 (Sinha et al., 2008)

6 Conclusions

Despite limitations in precision, the NanoSIMS technique is a novel and useful tool for the isotope analysis of individual atmospheric particles, the only technique capable of doing so. Given the range of S-isotopic ratios in aerosol bulk samples, the achievable precision and accuracy of a few permil for the measurement of the $^{34}S/^{32}S$ ratio in individual aerosol particles is sufficient to investigate physical and chemical processes related to aerosol formation and transport.

We found that contributions of SO_2 from marine biogenic sources in October 2005 were minor (~14%), and that formation of nss-sulfate was mainly through homogenous oxidation of SO_2 (70–100%). Heterogeneous oxidation in sea salt particles under clean conditions was more efficient in fine mode (~25%) than in coarse mode particles (~10%), and higher under polluted conditions (75% and 58%, respectively).

Acknowledgements. We thank Gerard Jennings and Colin O'Dowd from the Department of Physics, National University of Ireland, Galway, for their help and support during sample

collection at the Atmospheric Research Station Mace Head and for providing meteorological data. This research is funded by the Max Planck Society.

This Open Access Publication is financed by the Max Planck Society.

References

Alewell, C., Mitchell, M. J., Likens, G. E., and Krouse, R.: Assessing the origin of sulfate deposition at the Hubbard Brook Experimental Forest: Journal of Environmental Quality, 29, 759–767, 2000.

Alexander, B., Park, R. J., Jacob, D. J., Li, Q. B., Yantosca, R. M., Savarino, J., Lee, C. C. W., and Thiemens, M. H.: Sulfate formation in sea-salt aerosols: Constraints from oxygen isotopes, J. Geophys. Res.-Atmos., 110(D10), 307–319, doi:10.1029/2004JD005659, 2005.

Alexander, B., Park, R. J., Jacob, D. J., and Gong, S.: Transition metal catalyzed oxidation of atmpospheric sulfur: Global implications for the sulfur budget, J. Geophys. Res., in press, 2009.

Amelinckx, S., van Dycke, D., van Landuyt, J., and van Tendeloo, G.: Handbook of Microscopy: Applications in Materials Science, Solid-State Physics and Chemistry, Wiley-VCH, 1998.

Andreae, M. O., Charlson, R. J., Bruynseels, F., Storms, H., van Grieken, R., and Maenhaut, W.: Internal mixture of Sea salt, silicates, and excess sulfate in marine aerosols, Science, 232, 1620–1623, 1986.

Andreae, M. O. and Crutzen, P. J.: Atmospheric aerosols: Biogeochemical sources and role in atmospheric chemistry, Science, 276, 1052–1058, 1997.

Andreae, M. O., Jones, C. D., and Cox, P. M.: Strong present-day aerosol cooling implies a hot future, Nature, 435, 1187–1190, 2005.

Andronache, C., Chameides, W. L., Davis, D. D., Anderson, B. E., Pueschel, R. F., Bandy, A. R., Thornton, D. C., Talbot, R. W., Kasibhatla, P., and Kiang, C. S.: Gas-to-particle conversion of tropospheric sulfur as estimated from observations in the western North Pacific during

PEM-West B, J. Geophys. Res.-Atmos., 102(D23), 28 511–28 538, doi:10.1029/97JD01969, 1997.
Barrie, L. A., Yi, Y., Leaitch, W. R., Lohmann, U., Kasibhatla, P., Roelofs, G. J., Wilson, J., McGovern, F., Benkovitz, C., Melieres, M. A., Law, K., Prospero, J., Kritz, M., Bergmann, D., Bridgeman, C., Chin, M., Christensen, J., Easter, R., Feichter, J., Land, C., Jeuken, A., Kjellstrom, E., Koch, D., and Rasch, P.: A comparison of large-scale atmospheric sulfate aerosol models (COSAM): overview and highlights, Tellus B, 53, 615–645, 2001.
Baroni, M., Thiemens, M. H., Delmas, R. J., and Savarino, J.: Mass-independent sulfur isotopic compositions in stratospheric volcanic eruptions, Science, 315, 84–87, 2007.
Bauer, S. E. and Koch, D.: Impact of heterogeneous sulfate formation at mineral dust surfaces on aerosol loads and radiative forcing in the Goddard Institute for Space Studies general circulation model, J. Geophys. Res.-Atmos., 110(D17), 202–217, doi:10.1029/2005JD005870, 2005.
Benkovitz, C. M., Miller, M. A., Schwartz, S. E., and Kwon, O. U.: Dynamical influences on the distribution and loading of SO_2 and sulfate over North America, the North Atlantic, and Europe in April 1987, Geochem. Geophy. Geosy., 2, doi:10.1029/2000GC000129, 2001.
Berresheim, H., Elste, T., Tremmel, H. G., Allen, A. G., Hansson, H. C., Rosman, K., Dal Maso, M., Makela, J. M., Kulmala, M., and O'Dowd, C. D.: Gas-aerosol relationships of H_2SO_4, MSA, and OH: Observations in the coastal marine boundary layer at Mace Head, Ireland, J. Geophys. Res.-Atmos., 107(D19), 8100, doi:10.1029/2000JD000229 2002.
Borchert, H.: Principles of oceanic salt deposition and metamorphism, in: Chemical Oceanography Vol. 2., ed. by Riley, J. P. and Skirrow, G., Academic Press, London, 205–276, 1965.
Calhoun, J. A., Bates, T. S., and Charlson, R. J.: Sulfur isotope measurements of submicrometer sulfate aerosol-particles over the Pacific-Ocean, Geophys. Res. Lett., 18, 1877–1880, 1991.
Caron, F., Tessier, A., Kramer, J. R., Schwarcz, H. P., and Rees, C. E.: Sulfur and oxygen isotopes of sulfate in precipitation and lakewater, Quebec, Canada, Appl. Geochem., 1, 601–606, 1986.
Castleman, A. W., Munkelwitz, H. R., and Manowitz, B.: Isotopic studies of sulfur component of stratospheric aerosol layer, Tellus, 26, 222–234, 1974.
Charlson, R. J., Lovelock, J. E., Andreae, M. O., and Warren, S. G.: Oceanic phytoplankton, atmospheric sulfur, cloud albedo and climate, Nature, 326, 655–661, 1987.
Cox, R. A. and Penkett, S. A.: Oxidation of atmospheric SO_2 by products of ozone-olefin reac-

tion, Nature, 230, 321–322, 1971.
Dentener, F., Williams, J., and Metzger, S.: Aqueous phase reaction of HNO_4: The impact on tropospheric chemistry, J. Atmos. Chem., 41, 109–134, 2002.
Derda, M., and Chmielewski, A. G.: Determination of sulfur isotope ratios in coal combustion processes. Paper presented at the Sixth International Symposium & Exhibition on Environmental Contamination in Central & Eastern Europe and the Commonwealth of Independent States 1.–4. September 2003, Prague, Czech Republic., 2003.
Ding, T., Valkiers, S., Kipphardt, H., De Bievre, P., Taylor, P. D. P., Gonfiantini, R., and Krouse, H. R.: Calibrated sulfur isotope abundance ratios of three IAEA sulfur isotope reference materials and V-CDT with a reassessment of the atomic weight of sulfur, Geochim. Cosmochim. Ac., 65, 2433–2437, 2001.
Draxler, R. R., and Rolph, G. D.: HYSPLIT (HYbrid Single-Particle Lagrangian Integrated Trajectory) Model access via NOAA ARL READY Website: http://www.arl.noaa.gov/ready/hysplit4.html, NOAA Air Resources Laboratory, Silver Spring, MD, 2003.
Ebert, M., Weinbruch, S., Hoffmann, P., and Ortner, H. M.: Chemical characterization of North Sea aerosol particles, J. Aerosol. Sci., 31 613–632, 2000.
Ebert, M., Weinbruch, S., Rausch, A., Gorzawski, G., Helas, G., Hoffmann, P., and Wex, H.: The complex refractive index of aerosols during LACE 98 as derived from the analysis of individual particles, J. Geophys. Res.-Atmos., 107(D21), 8121, doi:10.1029/2000JD000195, 2002.
Eriksen, T. E.: Sulfur Isotope-Effects.1. Isotopic-Exchange Coefficient for Sulfur Isotopes ^{34}S-$^{32}S^-$ in the System SO_1(g)-HSO_3^-aq at 25, 35, and 45°C, Acta Chem. Scand., 26, 573–580, 1972a.
Eriksen, T. E.: Sulfur Isotope-Effects. 3. Enrichment of $^{34}S^-$ by Chemical Exchange between SO_2g and Aqueous-Solutions of SO_2, Acta Chem. Scand., 26, 975–979, 1972b.
Eugster, H. P., Harvie, C. E., and Weare, J. H.: Mineral equilibria in a 6-component seawater system, Na-K-Mg-Ca-SO_4-Cl-H_2O, at 25-degrees-C, Geochim. Cosmochim. Ac., 44, 1335–1347, 1980.
Feingold, G., Frost, G. J., and Ravishankara, A. R.: Role of NO_3 in sulfate production in the wintertime northern latitudes, J. Geophys. Res.-Atmos., 107, 4640, doi:10.1029/2002JD002288, 2002.
Fitzgerald, J. W.: Marine aerosols: A review, Atmos. Environ., 25, 533–545, 1991.
Foner, H. A. and Ganor, E.: The chemical and mineralogical composition of some urban atmo-

spheric aerosols in Israel, Atmos. Environ., 26B, 1083–1093, 1992.
Gröner, E., and Hoppe, P.: Automated ion imaging with the NanoSIMS ion microprobe, Appl. Surf. Sci., 252, 7148–7151, 2006.
Gwaze, P., Schmid, O., Annegarn, H. J., Andreae, M. O., Huth, J., and Helas, G.: Comparison of three methods of fractal analysis applied to soot aggregates from wood combustion, J. Aerosol. Sci., 37, 820–838, 2006.
Hoornaert, S., Godoi, R. H. M., and van Grieken, R.: Single particle characterization of the aerosol in the marine boundary layer and free troposphere over Tenerife, NE Atlantic, during ACE-2., J. Atmos. Chem., 46, 271–293, 2003.
Hoornaert, S., Van Malderen, H., and van Grieken, R.: Gypsum and other calcium-rich aerosol particles above the North Sea, Environ. Sci. Technol., 30 1515–1520, 1996.
Hoppe, P.: NanoSIMS: A new tool in cosmochemistry, Appl. Surf. Sci., 252, 7102–7106, 2006.
Hoppe, P., Mostefaoui, S., and Stephan, T.: NanoSIMS oxygen and sulfur isotope imaging of primitive solar system materials, Lunar Planet. Sci., 36, abstract #1301 (CD-ROM), 2005.
Horie, O. and Moortgat, G. K.: Decomposition pathways of the excreted Criegee intermediates in the ozonolysis of simple alkenes, Atmos. Environ., 25, 1881–1896, 1991.
Jacob, D. J.: Heterogeneous chemistry and tropospheric ozone, Atmos. Environ., 34, 2131–2159, 2000.
Jacob, D. J. and Hoffmann, M. R.: A dynamic model for the production of H^+, NO_3^-, and SO_4^{2-} in urban fog, J. Geophys. Res., 88, 6611–6621, 1983.
Kawamura, H., Matsuoka, N., Tawaki, S., and Momoshima, N.: Sulfur isotope variations in atmospheric sulfur oxides, particulate matter and deposits collected at Kyushu Island, Japan, Water Air Soil Pollut., 130, 1775–1780, 2001.
Keene, W. C. and Pszenny, A. A. P.: Comment on "Reactions at interfaces as a source of sulfate formation in sea-salt particles" (I), Science, 303, p. 628b, 2004.
Krouse, H. R. and Grinenko, V. A.: Stable isotopes : natural and anthropogenic sulfur in the environment (Vol. 43), Wiley, Chichester, p. 440, 1991.
Kulmala, M., Pirjola, U., and Makela, J. M.: Stable sulfate clusters as a source of new atmospheric particles, Nature, 404, 66–69, 2000.
Laskin, A., Gaspar, D. J., Wang, W. H., Hunt, S. W., Cowin, J. P., Colson, S. D., and Finlayson-Pitts, B. J.: Reactions at interfaces as a source of sulfate formation in sea-salt particles, Science, 301, 340–344, 2003.
Lee, Y. N. and Schwartz, S. E.: Kinetics of oxidation of aqueous sulfur(IV) by nitrogen dioxide.

Paper presented at the Fourth International Conference on Precipitation Scavenging, Dry Deposition, and Resuspension, Santa Monica, California, 1982.
Lelieveld, J. and Crutzen, P. J.: The Role of Clouds in Tropospheric Photochemistry, J. Atmos. Chem., 12, 229–267, 1991.
Leung, F. Y., Colussi, A. J., and Hoffmann, M. R.: Sulfur isotopic fractionation in the gas-phase oxidation of sulfur dioxide initiated by hydroxyl radicals, J. Phys. Chem. A, 105, 8073–8076, 2001.
Li, J., Anderson, J. R., and Buseck, P. R.: TEM study of aerosol particles from clean and polluted marine boundary layers over the North Atlantic, J. Geophys. Res.-Atmos., 108(D6), 4189, doi:10.1029/2002JD002106, 2003.
McArdle, N. C. and Liss, P. S.: Isotopes and Atmospheric Sulfur, Atmos. Environ., 29, 2553–2556, 1995.
McArdle, N. C., Liss, P. S., and Dennis, P.: An isotopic study of atmospheric sulfur at three sites in Wales and at Mace Head, Eire., J. Geophys. Res.-Atmos., 103, 31 079–31 094, doi:10.1029/98JD01664, 1998.
Mukai, H., Tanaka, A., Fujii, T., Zeng, Y. Q., Hong, Y. T., Tang, J., Guo, S., Xue, H. S., Sun, Z. L., Zhou, J. T., Xue, D. M., Zhao, J., Zhai, G. H., Gu, J. L., and Zhai, P. Y.: Regional characteristics of sulfur and lead isotope ratios in the atmosphere at several Chinese urban sites, Environ. Sci. Technol., 35, 1064–1071, 2001.
Nielsen, H.: Isotopic composition of the major contributors to atmospheric sulfur, Tellus, 26, 213–221, 1974.
Niemi, J. V., Tervahattua, H., Virkkulad, A., Hillamod, R., Teinilä, K., Koponene, I. K., and Kulmala, M.: Continental impact on marine boundary layer coarse particles over the Atlantic Ocean between Europe and Antarctica, Atmos. Res., 75, 301–321, 2005.
Novak, M., Kirchner, J. W., Groscheova, H., Havel, M., Cerny, J., Krejci, R., and Buzek, F.: Sulfur isotope dynamics in two Central European watersheds affected by high atmospheric deposition of SO_x, Geochim. Cosmochim. Acta, 64, 367–383, 2000.
Novak, M., Jackova, I., and Prechova, E.: Temporal Trends in the Isotope Signature of Air-Borne Sulfur in Central Europe, Environ. Sci. Technol., 35, 255–260, 2001.
Nriagu, J. O., Holdway, D. A., and Coker, R. D.: Biogenic Sulfur and the Acidity of Rainfall in Remote Areas of Canada, Science, 237, 1189–1192, 1987.
O'Dowd, C. D., Hämeri, K., Mäkelä, J., Väkeva, M., Aalto, P., de Leeuw, G., Kunz, G. J., Becker, E., Hansson, H. C., Allen, A. G., Harrison, R. M., Berresheim, H., Kleefeld, C.,

Geever, M., Jennings, S. G., and Kulmala, M.: Coastal new particle formation: Environmental conditions and aerosol physicochemical characteristics during nucleation bursts, J. Geophys. Res.-Atmos., D19, 8107, doi:10.1029/2000JD000206, 2002.

Ohizumi, T., Fukuzaki, N., and Kusakabe, M.: Sulfur isotopic view on the sources of sulfur in atmospheric fallout along the coast of the Sea of Japan, Atmos. Environ., 31, 1339–1348, 1997.

Ohizumi, T., Take, N., Moriyama, N., Suzuki, O., and Kusakabe, M.: Seasonal and spatial variations in the chemical and sulfur isotopic composition of acid deposition in Niigata Prefecture, Japan, Water Air Soil Poll., 131, 1679–1684, 2001.

Patris, N., Delmas, R. J., and Jouzel, J.: Isotopic signatures of sulfur in shallow Antarctic ice cores, J. Geophys. Res.-Atmos., 105(D6), 7071–7078, doi:10.1029/1999JD900974, 2000a.

Patris, N., Mihalopoulos, N., Baboukas, E. D., and Jouzel, J.: Isotopic composition of sulfur in size-resolved marine aerosols above the Atlantic Ocean., J. Geophys. Res.-Atmos., 105(D11), 14 449–14 457, doi:10.1029/1999JD901101, 2000b.

Penner, J. E., Andreae, M. O., Annegarn, H., Barrie, L. A., Feichter, J., Hegg, D. A., Jayaraman, A., Leaitch, W. R., Murphy, D., Nganga, J., and Pitari, G.: Aerosols, their direct and indirect effects, in: Climate Change 2001: The Third Assessment Report to the Intergovernmental Panel on Climate Change, ed. by Houghton, J. T., Ding, Y., Griggset, J. et al., Cambridge University Press, Cambridge, UK, and New York, USA, 2001.

Posfai, M., Anderson, J. R., Buseck, P. R., and Sievering, H.: Compositional variations of Sea-salt-mode aerosol-particles from the North-Atlantic, J. Geophys. Res.-Atmos., 100(D11), 23 063–23 074, doi:10.1029/1995JD01636, 1995.

Raab, M. and Spiro, B.: Sulfur isotope variations during seawater evaporation with fractional crystallization, Chem. Geol., 86, 323–333, 1991.

Riciputi, L. R. and Greenwood, J. P.: Analysis of sulfur and carbon isotope ratios in mixed matrices by secondary ion mass spectrometry: Implications for mass bias corrections, Int. J. Mass Spectrom., 178, 65–71, 1998

Rojas, C. M. and van Grieken, R. E.: Electron-microprobe characterization of individual aerosol-particles collected by aircraft above the southern bight of the North-Sea., Atmos. Environ., 26, 1231–1237, 1992

Rolph, G. D.: Real-time Environmental Applications and Display sYstem (READY) Website (http://www.arl.noaa.gov/ready/hysplit4.html), NOAA Air Resources Laboratory, Silver Spring, MD, 2003.

Saltzman, E. S., Brass, G., and Price, D.: The mechanism of sulfate aerosol formation: Chemical and sulfur isotopic evidence., Geophys. Res. Lett., 10, 513–516, 1983.
Sander, R., Crutzen, P. J., and von Glasow, R.: Comment on "Reactions at interfaces as a source of sulfate formation in sea-salt particles" (II), Science, 303, p. 628c, 2004.
Sanusi, A. A., Norman, A. L., Burridge, C., Wadleigh, M., and Tang, W. W., Determination of the S isotope composition of methanesulfonic acid, Anal. Chem., 78, 4964–4968, 2006.
Savoie, D. L., Arimoto, R., Keene, W. C., Prospero, J. M., Duce, R. A., and Galloway, J. N., Marine biogenic and anthropogenic contributions to non-sea-salt-sulfate in the marine boundary layer over the North Atlantic Ocean, J. Geophys. Res.-Atmos., 107(D18), 4356, doi:10.1029/2001JD000970, 2002.
Savarino, J., Romero, A., Cole-Dai, J., and Thiemens, M. H.: UV induced mass-independent sulfur composition in stratospheric volcanic eruptions, Geophys. Res. Lett., 30(D21), 2131, doi:10.1029/2003GL018134, 2003.
Seinfeld, J. H. and Pandis, S. N.: Atmospheric Chemistry and Physics, Wiley & Sons, New York, 1998.
Sievering, H., Lerner, B., Slavich, J., Anderson, J., Posfai, M., and Cainey, J.: O_3 oxidation of SO_2 in sea-salt aerosol water: Size distribution of non-sea-salt-sulfate during the First Aerosol Characterization Experiment (ACE 1), J. Geophys. Res.-Atmos., 104(D17), 21 707–21 717, doi:10.1029/1998JD100086, 1999.
Sinha, B. W., Hoppe, P., Huth, J., Foley, S., and Andreae, M. O.: Sulfur isotope analyses of individual aerosol particles in the urban aerosol at a central European site (Mainz, Germany), Atmos. Chem. Phys., 8, 7217–7238, 2008, http://www.atmos-chem-phys.net/8/7217/2008/.
Sobanska, S., Coeur, C., Maenhaut, W., and Adams, F.: SEM-EDX characterization of tropospheric aerosols in the Negev Desert (Israel), J. Atmos. Chem., 44, 299–322, 2003.
Stoyan, D.: Stochastik für Ingenieure und Naturwissenschaftler, Wiley-VCH, 1998.
Suhre, K., Andreae, M. O., and Rosset, R., Biogenic sulfur emissions and aerosols over the tropical South Atlantic. 2. One-dimensional simulation of sulfur chemistry in the marine boundary layer, J. Geophys. Res., 100, 11 323–11 335, 1995.
Tanaka, N., Rye, D. M., Xiao, Y., and Lasaga, A. C.: Use of stable sulfur isotope systematics for evaluating oxidation reaction pathways and in-cloud scavenging of sulfur-dioxide in the atmosphere, Geophys. Res. Lett., 21(D14), 1519–1522, doi:10.1029/1994GL00893, 1994.
Thode, H. G., Graham, R. L., and Ziegler, J. A.: A mass spectrometer and the measurement of

isotope exchange factors, Can. J. Res., B23, 40–47, 1945.
Tichomirowa, M., Haubrich, F., Klemm, W., and Matschullat, J.: Regional and temporal (1992–2004) evolution of air-borne sulphur isotope composition in Saxony, southeastern Germany, central Europe, Isotopes Environ. Health Stud., 43, 295–305, 2007.
Vogt, R., Crutzen, P. J., and Sander, R.: A mechanism for halogen release from sea-salt aerosol in the marine boundary layer, Nature, 383, 327–330, 1996.
von Glasow, R. and Crutzen, P. J.: Model study of multiphase DMS oxidation with a focus on halogens, Atmos. Chem. Phys., 4, 589–608, 2004, http://www.atmos-chem-phys.net/4/589/2004/.
von Glasow, R., Sander, R., Bott, A., and Crutzen, P. J.: Modeling halogen chemistry in the marine boundary layer: 2. Interactions with sulfur and the cloud-covered MBL, J. Geophys. Res.-Atmos., 107(D17), 4323, doi:10.1029/2001JD000943, 2002.
Warneck, P.: The relative importance of various pathways for the oxidation of sulfur dioxide and nitrogen dioxide in sunlit continental fair weather clouds, Phys. Chem. Chem. Phys., 1, 5471–5483, 1999.
Weber, R. J., Chen, G., Davis, D. D., Mauldin III, R. L., Tanner, D. J., Eisele, F. L., Clarke, A. D., Thornton, D. C., and Bandy, A. R.: Measurements of enhanced H_2SO_4 and 3–4 nm particles near a frontal cloud during the First Aerosol Characterization Experiment (ACE 1), J. Geophys. Res.-Atmos., 106(D20), 24 107–24 117, doi:10.1029/2000JD000109, 2001.
Winterholler, B., Hoppe, P., Andreae, M. O., and Foley, S.: Measurement of sulfur isotope ratios in micrometer-sized samples by NanoSIMS, Appl. Surf. Sci., 252, 7128–7131, 2006.
Winterholler, B., Hoppe, P., Andreae, M. O., and Foley, S.: Sulfur isotope ratio measurements of individual sulfate particles by NanoSIMS, Int. J. Mass Spectrom., 272, 63–77, 2008.
Xhoffer, C., Bernard, P., van Grieken, R., and van der Auwera, L.: Chemical characterization and source apportionment of individual aerosol-particles over the North-Sea and the English-Channel using multivariate techniques, Environ. Sci. Technol., 25, 1470–1478, 1991.
Zayani, L., Rokbani, R., and Trablesi-Ayedi, M.: Study of the evaporation of a brine involving the system Na^+, Mg^{2+}, K^+, Cl^-, SO_4^{2-}-H_2O-crystallization of oceanic salts, J. Therm. Anal. Calorim., 57, 575–580, 1999.
Zhang, Y. M., Mitchell, M. J., Christ, M., Likens, G. E., and Krouse, H. R.: Stable sulfur isotopic biogeochemistry of the Hubbard Brook Experimental Forest, New Hampshire, Biogeochemistry, 41, 259–275, 1998.
Zhao, F. J., Knights, J. S., Hu, Z. Y., and McGrath, S. P.: Stable sulfur isotope ratio indicates

long-term changes in sulfur deposition in the broadbalk experiment since 1845, J. Environ. Qual., 32, 33–39, 2003.
Zhuang, H., Chan, C. K., Fang, M., and Wexler, A. S.: Formation of nitrate and non sea-salt-sulfate on coarse particles, Atmos. Environ., 33, 4223–4233, 1999.

Table 1. Summary of all samples collected at Mace Head in October 2005.

Sample	Date	Flow [l/min]	Sample [m^3]	T_{min} [°C]	T_{max} [°C]	RH_{min} [%]	RH_{max} [%]	Windspeed [km/h]	Trajectory group	
Sample 1	30.09.–01.10.	20	26.5	9.6	14.1	69.1	88.7	29.9	A	clean
Sample 2	1.10.–02.10.	9.5	13.9	11.1	14.3	63.7	84.4	17.3	A	clean
Sample 3	2.10.–03.10.	4.5	5.4	12.1	14.3	63.3	82.6	12.1	B	clean
Sample 4	3.10.–04.10.	10	14.6	12.3	14.5	69.5	84.1	15.8	B	clean
Sample 5	4.10.–05.10.	10	13.8	12.6	15.4	70.9	85.8	13.0	C	polluted
Sample 6	5.10.–06.10.	12.5	12.7	12.3	13.9	82.0	89.6	13.5	C	polluted
Sample 7	Blank									
Sample 8	6.10.–07.10.	20	24.0	12.5	16.2	71.0	88.5	15.3	C	polluted
Sample 9	25.10–26.10.	21	27.8	11.7	15.3	82.3	97.5	18.5	D	clean
Sample 10	26.10–27.10.	20.5	28.8	15.0	16.8	75.1	97.2	19.7	D	clean
Sample 11	27.10–28.10.	30	42.1	11.2	15.6	71.0	97.7	21.6	D	clean
Sample 12	28.10–29.10.	30	40.3	10.6	13.9	67.5	95.9	16.7	D	clean
Sample 13	Blank									
Sample 14	29.10–30.10.	30.5	38.0	13.7	15.4	84.6	98.2	20.1	D	clean
Sample 15	Blank									
Sample 16	30.10–31.10.	30	39.6	10.4	14.8	65.5	87.3	21.7	D	clean

ACPD
9, 3307–3365, 2009

Table 2. Average semi-quantitative composition of different particle groups.

Group		N_a	NO_3	Na	Mg	Si	SO_4	Cl	K	Ca	Fe
Sea salt	1	5088	<0.1	38.7	0.7	<0.1	n.d.*	60.3	0.1	<0.1	n.d.
Aged sea salt	2	149	10.9	18.4	2.5	22.4	n.d.	38.0	0.7	5.4	2.3
Aged sea salt+S	2a	923	<0.1	34.6	2.3	0.7	15.2$^+$	45.7	0.1	1.0	0.1
Quartz and silicates	3	402	<0.1	2.5	0.5	94.9	n.d.	0.2	0.3	0.8	1.3
Silicates+S	3a	38	<0.1	5.4	0.1	35.2	51.2	0.1	0.6	2.2	6.7
Sodium nitrate	4	39	35.3	63.7	n.d.	n.d.	n.d.	0.2	n.d.	<0.1	n.d.
Sodium sulfate	4a	80	<0.1	28.0	0.1	n.d.	71.7	<0.1	n.d.	<0.1	n.d.
Magnesium sulfate	5	28	n.d.	0.1	26.8	n.d.	72.9	<0.1	n.d.	0.8	n.d.
Ammonium sulfate	6	276	<0.1	n.d.	n.d.	n.d.	99.9	<0.1	n.d.	<n.d.	n.d.
Gypsum	7	21	n.d.	0.2	n.d.	n.d.	77.4	n.d.	n.d.	22.4	n.d.
Mixed sulfates	8	83	1.3	10.4	3.1	4.7	67.2	6.0	3.7	3.5	0.2
Calcite/dolomite	9	185	<0.1	<0.1	n.d.	n.d.	n.d.	<0.1	n.d.	100	n.d.
Fe-oxides	10	64	n.d.	n.d.	n.d.	n.d.	n.d.	n.d.	n.d.	n.d.	100
Others	11	305	4.4	8.5	39.2	0.83	n.d.	0.36	23.06	2.7	0.9

* Sulfur content of this particle class is estimated based on NanoSIMS analysis as ~(8.5±1.3)%
$^+$ Sulfur content of this particle class is estimated based on NanoSIMS analysis as ~(18.8±2.9)% for "clean" samples and (29±4.4)% for "polluted" samples

ACPD
9, 3307–3365, 2009

Table 3. Instrumental mass fractionation factors for $^{34}S/^{32}S$ measured with the NanoSIMS and average diameter of the standard particles on which instrumental mass fractionation was determined. When the instrumental mass fractionation is determined on particles pressed into gold substrate, no grain size correction is necessary. $BaSO_{4\ true}$ is the calibrated isotope ratio of $BaSO_4$ based on delta values of 0.5‰ for IAEA SO-5 and 34.2‰ for IAEA SO-6 and a $n(^{34}S)/n(^{32}S)_{VCDT}$=0.044163 (Ding et al., 2001). $BaSO_{4\ SIMS}$ is the measured $N(^{34}S)/N(^{32}S)$-ratio measured by SIMS.

Session	$\frac{BaSO_{4\ true}}{BaSO_{4\ SIMS}}$	σ	$D_{P,m}$
Nov 2005	1.0148	0.0012	3.17
Apr 2006	1.0063	0.0003	4.0
May 2006	1.0232	0.0006	2.13
Jul 2006	1.0465	0.0004	1.7
Aug 2006	1.2320	0.0019	2.72

Table 4. Sample composition in % of total particle number (N_a) calculated from single particle analysis in the SEM. For fine mode filters, sulfate found during bulk analysis is generally higher than that found in single particle analysis. The contribution of this missing sulfate to total particle numbers is estimated, assuming a particle diameter of 150 nm.

Sample	1	2	3	4	5	6	8	9	10	11	12	14	16
Coarse mode filter sea salt+S<8.5% (1)	69.9	83.2	67	71.1	60.0	55.9	58.8	59.1	52.1	57.6	78.1	65.0	68.7
Aged sea salt (2)	0.6	1.5	0	0	1.7	1.7	1.8	9.0	3.3	2.1	1.96	3.6	2.6
+S (2a)	4.2	6.5	9	13.4	17.5	11.0	9.6	18.9	16.0	26.6	14.5	23.0	19.7
Quartz and silicates (3)	1.8	2.0	7	4.0	1.7	4.2	0.9	3.5	18.0	7.96	0.3	3.3	1.0
+ S (3a)	0	0	0	0	1.7	0	0.4	0	0.9	0.4	0	0	0
Sodium nitrate (4)	0	0	0	0	0	9.3	7.9	0.3	0.7	0.2	0.5	0.3	0
Sodium sulfate (4a)	2.5	0	0	0	2.5	1.7	2.2	0	0	0.5	0	0	0
Magnesium sulfate (5)	2.8	0	0	1.1	0	0.8	0.9	0.3	0.2	0	0.5	0	0
Ammonium(bi)sulfate (6)	8.2	1.5	2	5.6	7.5	0	0.9	3.1	0	1.7	0	0.6	0.2
Gypsum (7)	0	0	0	0	1.7	0	0.4	0	0	0	0.3	0.3	0
Mixed sulfates (8)	2.5	0.5	0	1.1	1.7	4.2	5.7	1.7	1.1	0.6	0.8	1.2	0.3
Calcite/dolomite (9)	1.6	1.5	6	2.3	1.7	5.9	2.2	0.3	0.2	1.4	0.3	1.2	4.2
Others (11)	5.9	3.5	9	3.4	2.5	5.1	8.3	3.5	7.6	1.0	2.7	1.5	3.4
N_a	680	202	100	177	120	118	228	286	551	1003	365	331	619
Fine mode filter													
Sea salt+S<8.5% (1)	79.2	65.0	39	57.5	4.7	4.1	6.3	74.5	18	72.8	66.3	2.8	54.1
Aged sea salt (2)	0.4	1.1		0	0	0	0.3	1.3	3	2.7	1.4	1.3	3.1
+S (2a)	5.0	10.6		5.5	0	0	1.3	3.3	9	4.5	2.8	3.6	6.1
Quartz and silicates (3)	4.4	1.7		6.8	7.1	3.1	5.6	2.6	6	7.2	4.8	4.3	4.1
+S (3a)	0.1	0.6		0	1.2	0	0.3	0	0	2.3	1.4	0.3	1.0
Sodium sulfate (4a)	0	0		2.7	30.6	11.3	20.6	0	6	0.2	2.6	0.5	0
Magnesium sulfate (5)	0	0		0	0	0	0	0	3	0	0	0	0
Ammonium sulfate* (6)	5.8	10.6	50	17.8	31.8	49.5	50.8	2.6	29	4.8	10.9	9.7	21.4
Gypsum (7)	0	0.6	0		0	0	1.3	0	0	0.4	1.4	0.5	0
Mixed sulfates (8)	0.3	0.6		1.4	1.2	1.0	0.3	0	0	1.1	1.0	0.3	0
Calcite/dolomite (9)	1.0	1.1		2.7	17.6	4.1	6.3	2.0	6	0.7	4.2	3.6	7.1
Fe-oxide (10)	2.6	4.4		2.7	2.4	4.1	0.3	0.7	9	1.6	1.2	1.8	2.0
Others (11)	1.2	3.9	13	2.7	3.4	22.7	6.3	13.1	12	1.8	1.8	1.5	1.0
N_a	722	180	8	73	85	97	301	153	34	559	496	393	98

ACPD
9, 3307–3365, 2009

Table 5. Chemical composition of Mace Head samples measured by ICP-OES analysis and derived from single particle analysis. All concentrations are given in ng/m^3. Blank filters were treated like samples throughout, but sampling time was only 1 s. The influence of filter blanks on the measured concentration was calculated using the average sample volume of 25.3 m^3. The coarse mode filters of samples 9, 10 and 11 were contaminated with silica gel pearls from the drier.

		ICP-OES									Single particle analysis								
		SO_4	Ca	K	Mg	Fe	Si	Al	Zn	Ba	NO_3	Na	Cl	SO_4	Ca	K	Mg	Fe	Si
Sample 1	coarse	281	66	45	133	<0.3	12	1.1	1.2	0.8	2	1570	2319	917	48	75	177	5	31
Sample 2	coarse	346	71	47	149	1.2	13	<1.2	4.0	0.4	0.2	1402	2139	434	42	35	71	11	26
Sample 3	coarse	453	74	53	180	<1.5	38	<2.9	4.2	3.6		2544	3516	913	117	147	301	14	141
Sample 4	coarse	214	44	37	110	<0.5	<8	<1.1	0.8	1.2		1375	2004	541	25	17	63	3	27
Sample 5	coarse	396	52	38	110	<0.6	<9	<1.2	0.7	<0.4	15	480	737	447	26	9	45	3	614
Sample 6	coarse	473	64	44	109	<0.6	<9	<1.3	2.6	0.1	220	1451	1639	664	59	76	196	4	26
Blank	coarse	<71	1	2	1	<0.3	<5	3.9	0.4	<0.2									
Sample 8	coarse	405	51	45	112	0.7	<5	<0.3	0.5	<0.2	453	1281	1395	538	536	71	170	6	17
Sample 9	coarse	65	27	18	41	0.9	<4	0.4	4.2	<0.2	31	835	1319	287	25	37	77	11	50
Sample 10	coarse	200	29	26	65	0.9	<4	<0.6	0.4	<0.2	29	1125	1629	304	25	536	123	13	122
Sample 11	coarse	116	19	19	49	0.4	<3	0.4	0.3	0.2	5	902	1317	335	24	9	29	4	42
Sample 12	coarse	143	9	12	27	<0.2	<3	<0.2	0.1	0.1	10	477	737	211	14	41	91	2	7
Blank	coarse	<71	0.2	1	<1	<0.3	<5	<0.3	<0.5	<0.2									
Sample 14	coarse	149	24	23	63	<0.2	<3	<0.4	<0.3	<0.1	6	1200	1782	378	33	20	61	5	33
Blank	coarse	<71	<1	<1	2	<0.3	<5	<0.3	<0.5	<0.2									
Sample16	coarse	180	22	19	54	<0.2	<3	<0.4	<0.3	<0.2	20	1406	2149	467	75	31	106	5	22
Sample 1	fine	402	41	35	97	<0.3	<5	<0.6	1.9	2.8		901	1351	259	16	62	123	14	14
Sample 2	fine	294	23	23	46	<0.6	<9	3.4	0.6	<0.4		319	480	136	9	12	24	7	2
Sample 3	fine	331	<1	0.4	10	<1.5	<22	4.7	<2.2	<1.1		108	165	59	23	3	7	1	7
Sample 4	fine	222	<1	8	28	<0.5	<8	<1.1	<0.8	2.8		160	233	74	7	1	65	1	5
Sample 5	fine	243	<1	4	11	<0.6	<9	<1.2	<0.9	2.3		19	16	43	11	3	5	1	2
Sample 6	fine	322	16	<1	15	<0.6	<9	<1.3	<0.9	<0.5		26	1	69	2	8	14	4	6
Blank fine	<71	<1	<1	<1	<0.3	<5	<0.6	0.5	1.9										
Sample 8	fine	1580	17	28	45	<0.3	<5	0.7	0.9	<0.3		359	265	779	71	24	646	7	30
Sample 9	fine	153	24	25	59	<0.3	<4	<0.6	<0.4	<0.2		545	847	176	9	14	34	6	4
Sample 10	fine	106	<1	3	4	<0.3	<4	<0.6	<0.4	<0.2		8	9	13	3	6	14	3	5
Sample 11	fine	223	21	24	57	<0.2	<3	0.4	<0.3	<0.1		962	1469	427	26	76	29	17	98
Sample 12	fine	174	18	18	43	<0.2	<3	<0.4	<0.3	<0.1		232	345	126	13	2	8	5	7
Blank	fine	<71	<1	<1	2	<0.3	<5	<0.6	<0.5	<0.2									
Sample 14	fine	186	16	17	43	<0.2	<3	<0.4	0.8	<0.2		366	561	127	8	3	11	5	10
Blank	fine	<71	3	<1	<1	<0.3	<5	<0.6	<0.5	0.1									
Sample 16	fine	155	7	8	21	<0.2	<3	<0.4	<0.3	<0.2		174	272	55	22	3	8	1	4

ACPD
9, 3307–3365, 2009

Table 6. Average isotopic composition of all particles of a particular chemical composition derived from single particle analysis in the NanoSIMS. f_{SO_4} denotes the fraction that the respective particle type contributed to total sulfate in the sample. Errors are 1σ and include the standard deviation of the isotopic composition caused by the presence of different oxidation pathways in separate particles within the same particle group, i.e., the error of the weighted mean is multiplied by sqrt(χ^2) for χ^2>1 and, therefore, includes the natural variability of the sample.

	Sample 1 clean $\delta^{34}S_{VCDT}$ [‰]	f_{SO_4}	Sample 2 clean $\delta^{34}S_{VCDT}$ [‰]	f_{SO_4}	Sample 3 clean $\delta^{34}S_{VCDT}$ [‰]	f_{SO_4}	Sample 4 clean $\delta^{34}S_{VCDT}$ [‰]	f_{SO_4}	Sample 6 polluted $\delta^{34}S_{VCDT}$ [‰]	f_{SO_4}
Sea salt+S (1)	23±7	0.412		0.507	24±7	0.409	21±3	0.395	22±6	0.225
Aged sea salt+S (2a)	15±1	0.041	19±1	0.100	23±12	0.237	18±4	0.119	11±4	0.230
Quartz+S (3a)		0.004	6±6	0.001		0		0		0
Sodium sulfate (4a)		0.039		0		0		0.009	4±7	0.114
Magnesium sulfate (5)	23±7	0.047		0		0	25±18	0.018		0.058
Ammonium sulfate (6)	5±3	0.308	1±7	0.356		0.355	−9±4	0.324		0.271
Gypsum (7)	14±7	0.001		0.001		0		0.008		0
Mixed sulfates (8)	12±4	0.148	5±15	0.036		0	2±5	0.127	6±4	0.103
$\delta^{34}S_{VCDT}$ bulk	15±3		13±3		13±4		8±2		7±2	
SO_4^{2-} [μg m^{-3}]	1.319		0.728		1.244		0.763		0.986	
nss SO_4^{2-} [μg m^{-3}]	0.687		0.322		0.677		0.413		0.698	
f_{nsss}	0.52		0.44		0.54		0.54		0.71	
f_{het}	0.12±0.08		0.06±0.01		0.27±0.09		0.07±0.05		0.28±0.07	

	Sample 8 polluted $\delta^{34}S_{VCDT}$ [‰]	f_{SO_4}	Sample 9 clean $\delta^{34}S_{VCDT}$ [‰]	f_{SO_4}	Sample 10 clean $\delta^{34}S_{VCDT}$ [‰]	f_{SO_4}	Sample 11 clean $\delta^{34}S_{VCDT}$ [‰]	f_{SO_4}	Sample 16 clean $\delta^{34}S_{VCDT}$ [‰]	f_{SO_4}
Sea salt+S (1)		0.107		0.566	22±3	0.435	22±7	0.446	19±2	0.471
Aged sea salt+S (2a)	19±5	0.058		0.232	9±3	0.231	3±3	0.236	7±2	0.323
Quartz+S (3a)	11±6	0.008		0		0.024		0.023		0.00.1
Sodium sulfate (4a)	8±7	0.107		0		0.005		0.015		0
Magnesium sulfate (5)		0.010		0.006		0.031		0.018		0
Ammonium sulfate (6)		0.636		0.165	−4±6	0.229		0.183		0.195
Gypsum (7)	19±6	0.017		0		0		0.009		0
Mixed sulfates (8)	13±6	0.056	2±3	0.033	1±9	0.045		0.069	−4±5	0.010
$\delta^{34}S_{VCDT}$ bulk	1±2				11±2		9±4		10±1	
SO_4^{2-} [μg m^{-3}]	2.118		0.463		0.410		0.762		0.622	
nss SO_4^{2-} [μg m^{-3}]	1.782		0.147		0.160		0.309		0.258	
f_{nsss}	0.84		0.32		0.39		0.41		0.42	
f_{het}	0.24±0.06				−0.05±0.13		−0.14±0.19		0.11±0.11	

Table 7. Nss-sulfate composition and relative importance of different oxidation pathways for sea salt particles.

	Coarse filter				Fine filter				6/3a*	Other particles
	6/3a* [‰]	$SO_{4\,hom}$ [‰]	$SO_{4\,het}$ [‰]	f_{het} [%]	6/3a* [‰]	$SO_{4\,hom}$ [‰]	$SO_{4\,het}$ [‰]	f_{het} [%]	SO_2 [‰]	SO_2 [‰]
Filter 1		−5±3	24±8	4±29	5±3	7±2		4±5	14±3	12±4
Filter 2	6±6	−9±5	22±3	1±11	1±7	−6±4	29±3	3±4	13±5	10±4
Filter 3		−7±6	31±4	35±16						11±6
Filter 4	−9±6	−6±2	32±4	6±15	−9±7		17±6	11±15	0±4	5±4
Filter 6		−7±2	20±2	39±21		−13±8	28±6	14±9		3±1
Filter 8		−6±3	19±2	37±11						3±2
Filter 9		−1±3								8±3
Filter 10	−4±6	−7±2		5±30		−6±8		0±12	5±6	2±2
Filter 11		−9±3		0±34				0±28		0±3
Filter 16		−4±3	16±4	0±14		−8±3		1±2		3±2

*Ammonium sulfate/sulfuric acid particles and sulfuric acid condensed on quartz particles

ACPD
9, 3307–3365, 2009

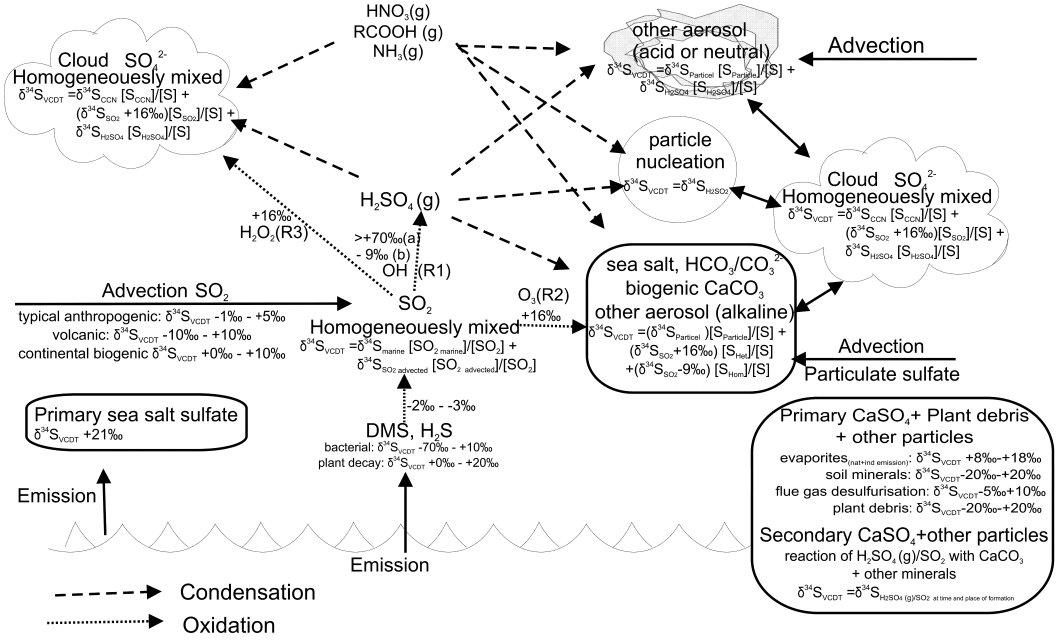

Fig. 1. Sulfur isotope chemistry of SO_2 and sulfate aerosol in the marine boundary layer.

ACPD
9, 3307–3365, 2009

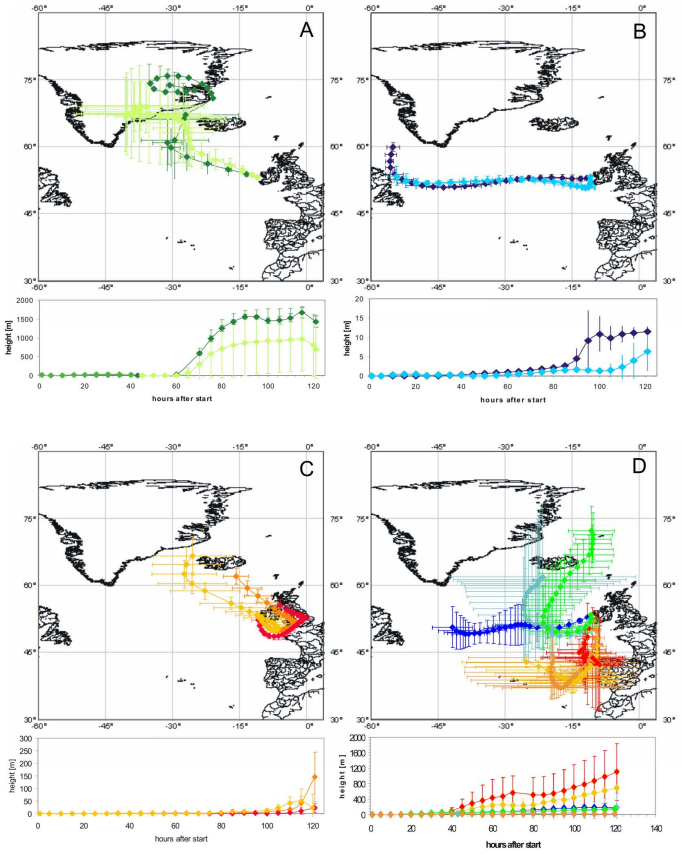

Fig. 2. Backward trajectories, calculated using the vertical motion mode in the HYSPLIT4 (HYbrid Single-Particle Lagrangian Integrated Trajectory) model with the FNL meteorological database at NOAA Air Resources Laboratory's web. Samples are grouped into 4 groups based on back trajectories, local meteorological data and aerosol composition. Several back trajectories were calculated for every 2 h during the sampling time interval, and error bars of the trajectories represent the standard deviation of different trajectories calculated for the same sample.

ACPD
9, 3307–3365, 2009

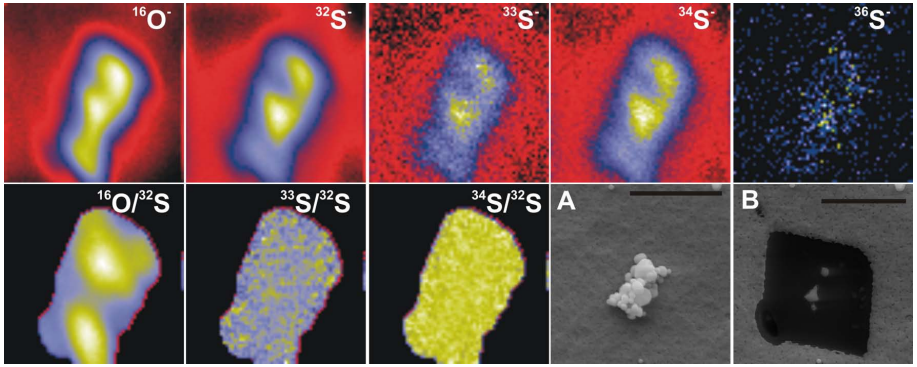

Fig. 3. $BaSO_4$ standard grain illustrating the analytical procedure. Particles are documented with the help of the SEM before **(A)** and after SIMS analysis **(B)**. SEM conditions: EHT 10 keV, WD 9 mm, scale bar 2 µm. NanoSIMS: simultaneous collection of $^{16}O^-$, $^{32}S^-$, $^{33}S^-$, $^{34}S^-$ and $^{36}S^-$ ion images, field of view 2 µm×2 µm, Cs^+ primary ions, 1 pA primary current, 100 nm beam diameter. The black square in the SEM image **(B)** is the area were the filter material was sputtered away during NanoSIMS analysis and indicates the exact position of the measurement field.

ACPD
9, 3307–3365, 2009

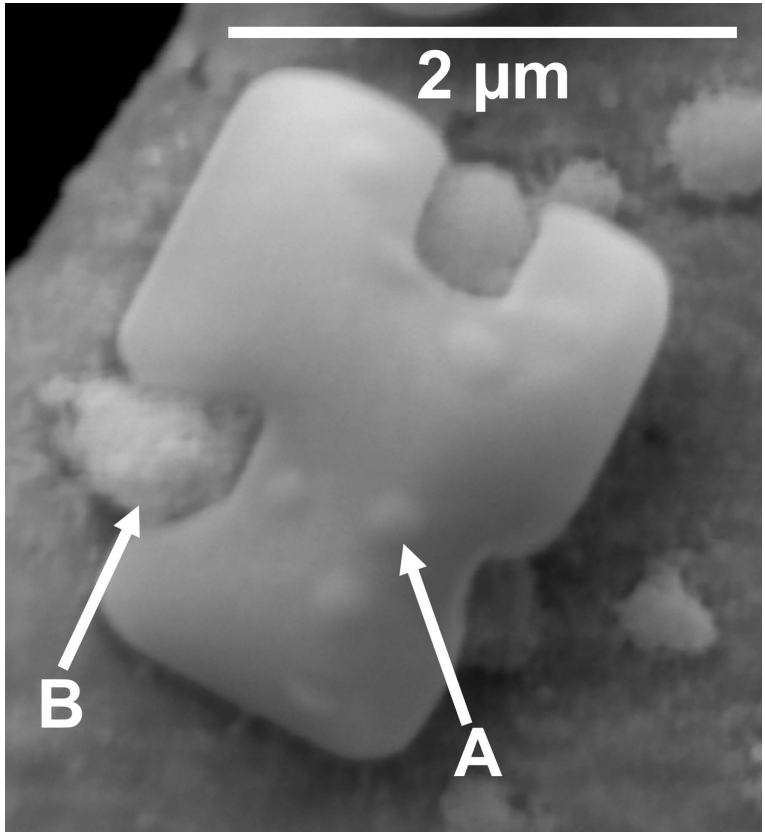

Fig. 4. Sea salt particle showing various stages of reaction with sulfuric acid. **(A)** initial stage of chlorine depletion. The particle surface shows traces of reactions, similar to those observed by Laskin et al. (2003) after reaction of NaCl with OH(g). **(B)** Later stage of chlorine depletion shows formation of separate regions consisting of mixed sulfates (Na, Mg) within the NaCl crystal.

ACPD
9, 3307–3365, 2009

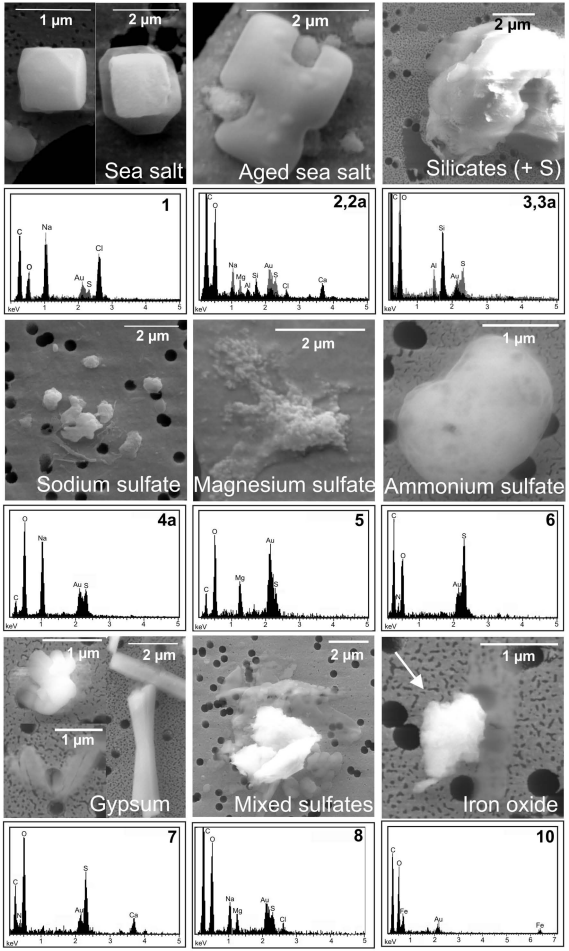

Fig. 5. SEM images and typical EDX spectra for all particle groups (except groups 4 and 9).

ACPD
9, 3307–3365, 2009

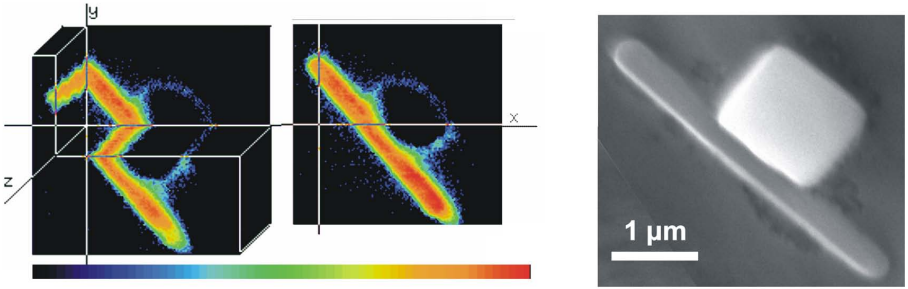

Fig. 6. 3-D secondary ion image of $^{32}S^-$ of a sea salt particle and SEM image of the same particle. SEM conditions: EHT 15 keV, WD 9 mm. NanoSIMS: field of view 4 µm×4 µm, 20 planes, Cs^+ primary ions, 1 pA primary current, 100 nm beam diameter.

ACPD
9, 3307–3365, 2009

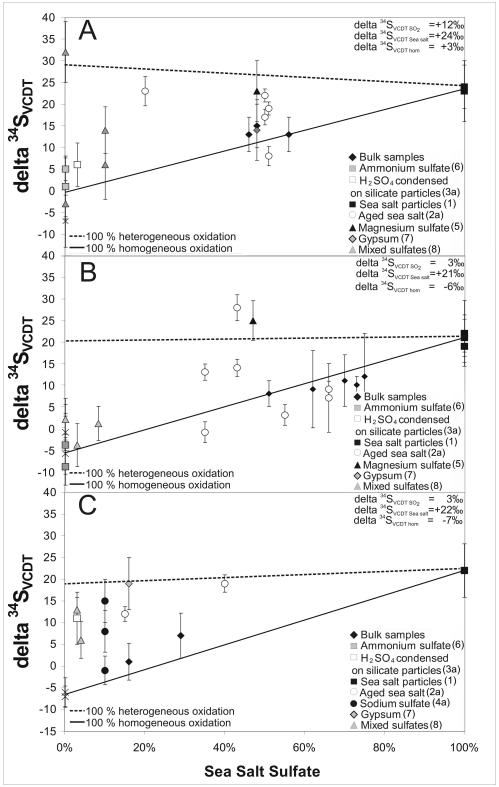

Fig. 7. Isotopic composition against sea-salt-sulfate content (δ^{34}S) of bulk samples and different particle groups (1–8). Samples from the "clean" samples with similar source SO_2 are grouped together in one panel each (**A** and **B**). Polluted samples were put into a separate plot **(C)**, values for coarse and fine fraction are plotted seperately. The solid line represents the mixing line between sea-salt-sulfate and nss-sulfates from homogeneous oxidation, the dashed line connects nss-sulfates derived from heterogeneous oxidation and sea-salt-sulfate. The vertical distance of a particle group to the mixing line between sea salt and ammonium sulfate (solid line) gives the contribution of heterogeneous oxidation to the respective particle group/sample. The symbol × stands of the calculated nss-sulfate composition from homogeneous oxidation for samples, for which no ammonium sulfate particles were analyzed successfully.

ACPD
9, 3307–3365, 2009

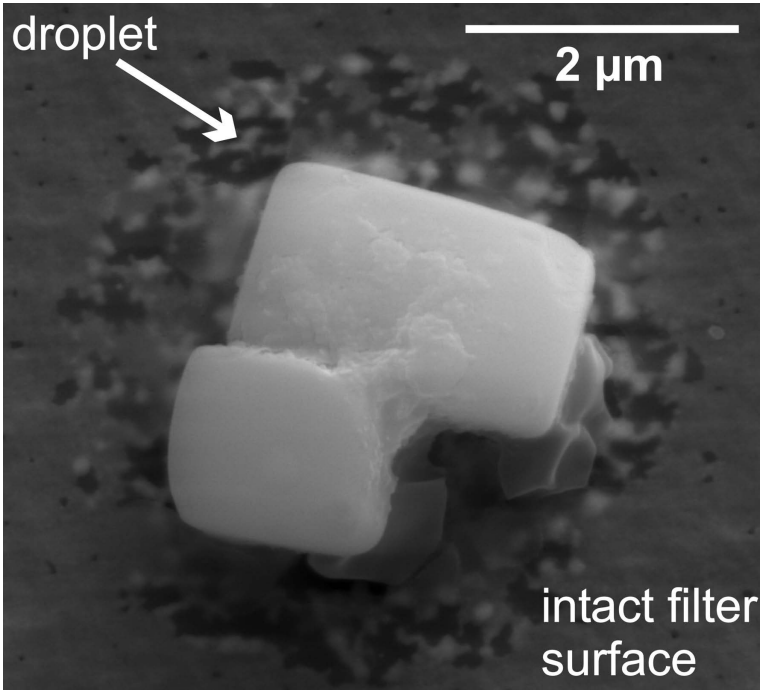

Fig. 8. SEM image of a particle and the surrounding droplet on the Nuclepore filter. Where the droplet touched the filter, the gold coating of the filter is damaged. SEM conditions: EHT 10 keV, WD 9 mm.

ACPD
9, 3307–3365, 2009